iScience

CellPress
OPEN ACCESS

Article

Semaphorin3C identified as mediator of neuroinflammation and microglia polarization after spinal cord injury

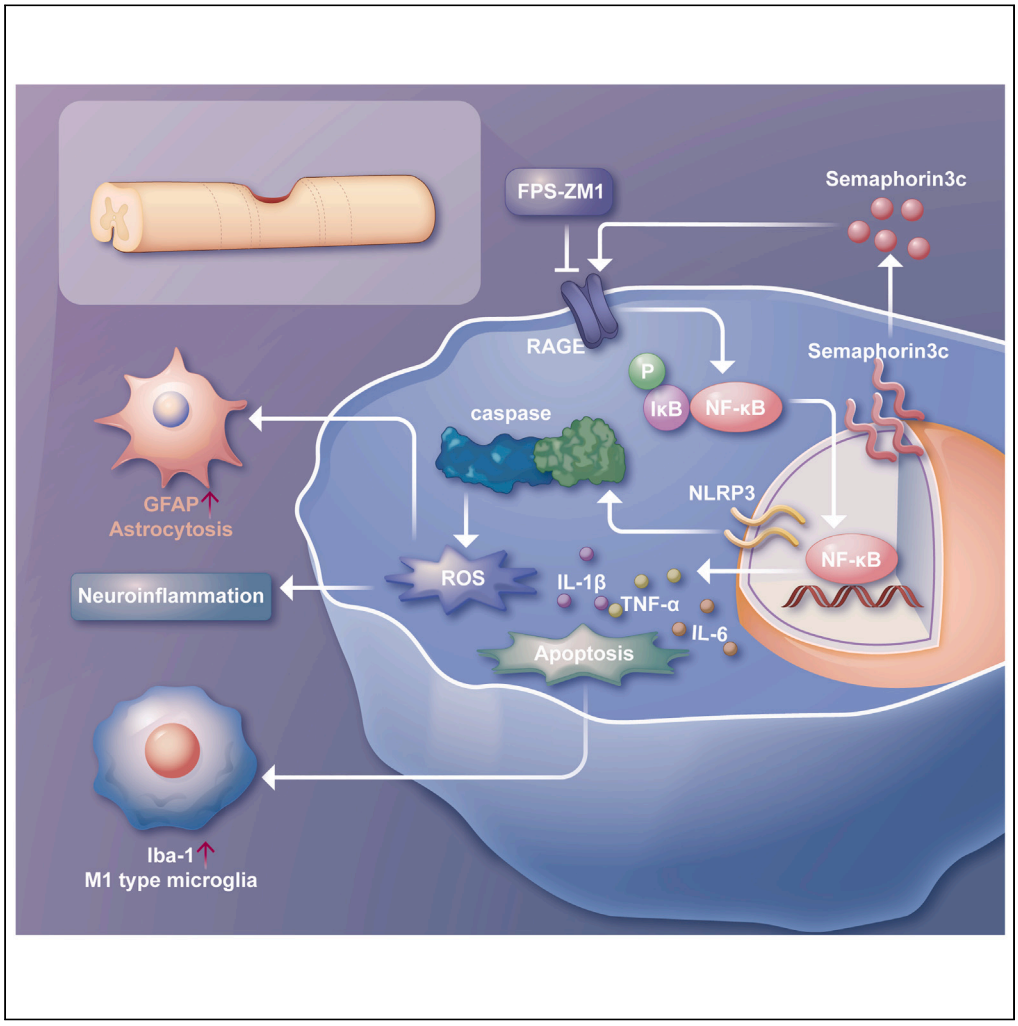

Junjie Shen, Liangzhi Gong, Yi Sun, ..., Bingbo Bao, Yun Qian, Xianyou Zheng

bingbobao@163.com (B.B.)
lollipopcloudland@foxmail.com (Y.Q.)
zhengxianyou@126.com (X.Z.)

Highlights

SEMA3C expressed in microglia/macrophages enhances neuroinflammation in mouse SCI

RAGE-NFkB signaling is activated in SEMA3C-mediated neuroinflammation

FPS-ZM1 saved axons by suppressing SEMA3C-mediated secondary neuroinflammatory damage

This is the first known demonstration of SEMA3C involvement in SCI neuroinflammation

Shen et al., iScience 27, 109649
May 17, 2024
https://doi.org/10.1016/j.isci.2024.109649

iScience

CellPress
OPEN ACCESS

Article

Semaphorin3C identified as mediator of neuroinflammation and microglia polarization after spinal cord injury

Junjie Shen,[1,2] Liangzhi Gong,[1,2] Yi Sun,[1] Junqing Lin,[1] Wencheng Hu,[1] Jiabao Wei,[1] Xin Miao,[1] Tao Gao,[1] Jinlong Suo,[1] Jia Xu,[1] Yimin Chai,[1] Bingbo Bao,[1,*] Yun Qian,[1,*] and Xianyou Zheng[1,3,*]

SUMMARY

Excessive neuroinflammation after spinal cord injury (SCI) is a major hurdle during nerve repair. Although proinflammatory macrophage/microglia-mediated neuroinflammation plays important roles, the underlying mechanism that triggers neuroinflammation and aggravating factors remain unclear. The present study identified a proinflammatory role of semaphorin3C (SEMA3C) in immunoregulation after SCI. SEMA3C expression level peaked 7 days post-injury (dpi) and decreased by 14 dpi. *In vivo* and *in vitro* studies revealed that macrophages/microglia expressed SEMA3C in the local microenvironment, which induced neuroinflammation and conversion of proinflammatory macrophage/microglia. Mechanistic experiments revealed that RAGE/NF-κB was downstream target of SEMA3C. Inhibiting SEMA3C-mediated RAGE signaling considerably suppressed proinflammatory cytokine production, reversed polarization of macrophages/microglia shortly after SCI. In addition, inhibition of SEMA3C-mediated RAGE signaling suggested that the SEMA3C/RAGE axis is a feasible target to preserve axons from neuroinflammation. Taken together, our study provides the first experimental evidence of an immunoregulatory role for SEMA3C in SCI via an autocrine mechanism.

INTRODUCTION

Spinal cord injury (SCI) is a central nervous system (CNS) condition that causes widespread motor, sensory, and autonomic dysfunction mediated by nerves below the level of the spinal injury. SCI is associated with a high disability rate and results in a heavy burden on patients, families, and society.[1] Conventional treatment such as pharmacological and surgical inventions available are not curative and only aim to mitigate symptoms, mainly because they do not target the complex pathological and physiological processes that unfold after SCI.[2,3] Given the significant global prevalence of SCI, it is imperative to identify, elucidate, and delineate the pathological mechanisms involved in SCI, with the goal of developing novel effective therapies that target-specific pathophysiological mechanisms and improve the quality of life of sufferers.

It is well known that secondary injury disrupts the local microenvironment around the lesion and causes other endogenous obstacles to self-repair after SCI.[4] Secondary injury after SCI is initiated by an inflammatory response mediated by an imbalance in the expression of M1/M2 macrophages/microglia immediately after the injury.[5] Macrophages/microglia become polarized toward the toxic M1 phenotype, which induces neuroinflammation and activates astrocytes.[6,7] A cascade of inflammation events leads to tissue edema, neuronal apoptosis, resulting in neural damage. This facilitates extravasation of immune cells, contributing to a persistent and chronic proinflammatory state.[8] Although having knowledge of the role of proinflammatory macrophage/microglia-mediated neuroinflammation is important for understanding SCI and developing restorative treatments, the mechanism(s) and molecules responsible for triggering the inflammatory response following SCI and the aggravating factors remain unclear.[9]

Semaphorin3C (SEMA3C) is a 85 kDa glycoprotein that belongs to the family of semaphorins, which were first identified to be nerve repellent factors involved in axon guidance.[10] The SEMA3 family differs from other vertebrate semaphorins in that they are the only semaphorin proteins that are secreted; the others are bound to the cell membrane or span the membrane.[11,12] Since its initial characterization as an axon guidance factor, SEMA3C was found to be differentially expressed in acute kidney injury, cardiovascular abnormalities, and spinal cord development[13,14] as well as spinal cord injury.[15,16] Recent studies have revealed parallels between the nervous and immune systems in which axon guidance molecules can also function during normal immunological processes and can play a role in certain disorders like hepatocellular carcinoma.[17] Among the SEMA3 proteins, SEMA3A displayed immunomodulatory functions in responsive cell types.[18] The immunomodulatory

[1]Department of Orthopedic Surgery, Shanghai Sixth People's Hospital Affiliated to Shanghai Jiao Tong University School of Medicine, Shanghai 200233, P.R. China
[2]These authors contributed equally
[3]Lead contact
*Correspondence: bingbobao@163.com (B.B.), lollipopcloudland@foxmail.com (Y.Q.), zhengxianyou@126.com (X.Z.)
https://doi.org/10.1016/j.isci.2024.109649

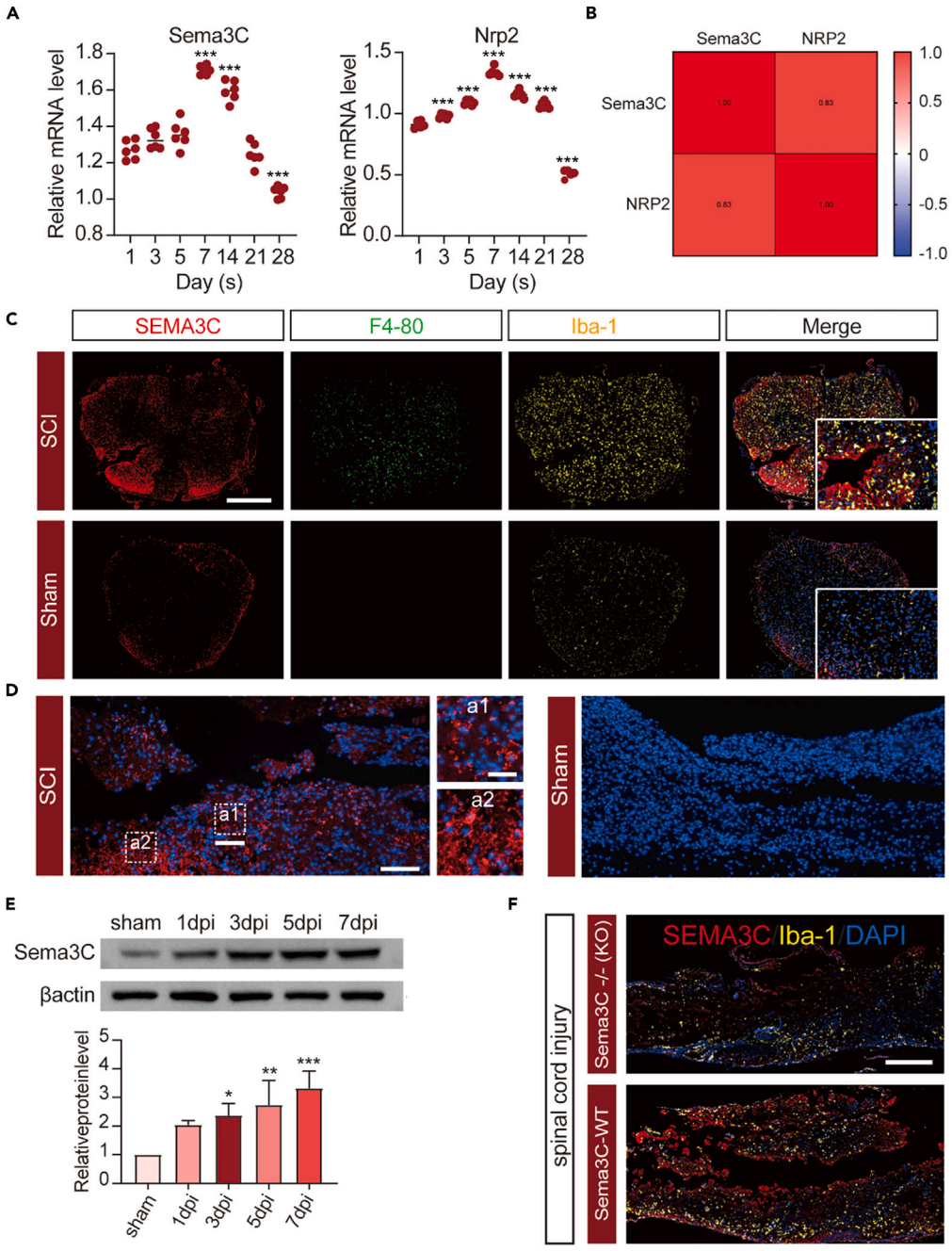

Figure 1. Semaphorin3C (SEMA3C) expression in mouse spinal cord after blunt-force SCI

(A) Temporal profile (indicated as days post-injury [dpi]) of SEMA3C mRNA expression (real-time qPCR) and mRNA expression of its receptor Nrp2 in spinal cord of SCI mice, relative to levels in control mice receiving sham injury. Black horizontal lines superimposed on individual data points indicate mean values on each day (sometimes obscured). Significant differences were evaluated by one-way ANOVA and post hoc Dunnett's tests for all panels; ***$p < 0.001$ versus 1 dpi group. For Sema3C analysis, $n = 6$. F (6, 35) = 88.73, R squared = 0.9383, p value < 0.0001 in ANOVA summary. For Nrp2 analysis, $n = 5$ in day 28 group and $n = 6$ in other groups. F (6, 34) = 483.5, R squared = 0.9884, p value <0.0001 in ANOVA summary.

(B) Heatmap of Pearson's correlation coefficients of SEMA3C mRNA and Nrp2 mRNA levels. Red shade indicates r = 1.0; white indicates r = 0; blue shade indicates r = −1.0.

(C) Epifluorescent images of spinal cord transverse sections from SCI (top) and sham-operated (bottom) mice triple immunostained for SEMA3C (red), F4-80 (green), and Iba1 (yellow) at 3 days after SCI (3 dpi). Sections counterstained with the nuclear stain DAPI (blue) reveal the location of all cells. Insets in merged images show higher magnification of staining in the same sections. SEMA3C appears to co-localize with macrophages (inset) around the lesion core in the spinal cord. $n = 3$. Scale bar, 400 μm.

Figure 1. *Continued*

(D) SEMA3C mRNA expression at the lesion core at 7 dpi, as detected by *in situ* hybridization. $n = 3$. Low magnification scale bar, 200 μm; high magnification scale, 50 μm.

(E) SEMA3C protein expression at the lesion site detected by western blotting and was quantified (data are represented as mean ± SD). Significant differences among groups in panel E were evaluated by one-way ANOVA and post hoc Dunnett's tests for all panels; $^{*}p < 0.05$; $^{**}p < 0.01$; and $^{***}p < 0.001$ versus the sham-operated control group ($n = 3$ mice per group). F (4, 10) = 8.489, R squared = 0.7725, p value = 0.0030 in ANOVA summary.

(F) Immunofluorescence staining for SEMA3C (red) and Iba1 (yellow) marker of lesion core at 3 dpi in SEMA3C-KO or WT mice. $n = 3$. Scale bar, 400 μm.

role of other SEMA3C proteins is less well characterized. In particular, SEMA3C is involved in chronic inflammation,[19] but its potential role in SCI and neuroinflammation remains unclear.

In the present study, we have expanded our understanding of the role of "immune semaphorins" in SCI. We provide evidence that SEMA3C has a role in mediating neuroinflammation in SCI. We first identified the temporal profile of SEMA3C expression from proinflammatory macrophages/microglia around the core of spinal cord lesions. Our *in vivo* and *in vitro* studies revealed that SEMA3C amplified the secondary injury after SCI via induction of neuroinflammation. This then polarizes proinflammatory macrophages/microglia and suppresses angiogenesis in an autocrine fashion. We also provide evidence for a mechanism. *In vivo* and *in vitro* experiments suggested that activation of the RAGE/NF-κB signaling pathway was responsible for SEMA3C-mediated inflammation. Using FPS-ZM1, an inhibitor of RAGE, we found that SEMA3C-related neuroinflammation and macrophage/microglia polarization were inhibited. Thus, axonal preservation after SCI was improved after this treatment *in vivo*. Our study identified a role that nerve-repellent factors play in SCI and deepened the understanding of complex neuroinflammation mechanisms secondary to SCI. These findings have clinical implications for approaches aimed at repairing SCIs.

RESULTS

SEMA3C expression is upregulated following SCI

We first assessed the temporal and spatial expression of SEMA3C in mouse spinal cord samples after SCI. To more closely model human SCI, we employed the Allen spinal cord contusion model.[20,21] Most human SCIs result from blunt-force trauma.[22] This model produces injuries that are more like human SCI than injuries observed in cord transection models; thus, we reasoned that it was appropriate to use the Allen model to answer our research question.[23]

After SCI was induced in our experiments, mRNA levels of SEMA3C and its classic receptor, Nrp2, increased considerably in the spinal cord during the first 2 weeks after injury, reaching the highest level 7 dpi (Figure 1A). By 14 dpi, SEMA3C and Nrp2 mRNA levels started to decrease, reaching control levels by 28 dpi. Pearson's correlation of SEMA3C and Nrp2 mRNA levels showed that their expression changed in parallel over time (r = 0.83; Figure 1B). Previous research showed that as secondary pathological events unfold in the injured spinal cord, microglia numbers in the cord peak by 7 dpi and decrease by 14 dpi.[24,25] As changes in SEMA3C expression paralleled changes in the microglial population in the spinal cord, we hypothesized that SEMA3C may be expressed by macrophages/microglia in the spinal cord.

In spinal cord sections obtained at 7 dpi, triple-fluorescent labeling for SEMA3C, Iba-1, and F4-80, the latter as macrophage marker,[26] appeared to show co-localization around the lesion core (Figure 1C). The sham-operated group (set as control) showed weak fluorescence intensity. The expression of SEMA3C was further confirmed by *in situ* hybridization, western blot, and immunofluorescence staining in Sema3C-KO mice. In the spinal cord injury group, significant Sema3C mRNA-positive signals were detected along the lesion core when compared to the sham injury group (Figure 1D). Expression level of SEMA3C protein at different time points was detected by Western blot (Figure 1E). The Western blot result showed a marked increase in SEMA3C expression over time, which was consistent with real-time qPCR analysis. In addition, immunofluorescence staining of SEMA3C/Iba-1 confirmed no detection of nonspecific antigens in WT and KO mice (Figure 1F).

SEMA3C-induced neuroinflammation and cell apoptosis after SCI

Given the observation that SEMA3C was expressed around the lesion core after SCI for at least 7 dpi, an obvious question is whether this expression of SEMA3C, and subsequent increase in SEMA3C levels around the lesion core, had cellular consequences. Therefore, we performed *in vitro* and *in vivo* experiments to determine the possible pathological effects of SEMA3C protein administration around the lesion after SCI.

Possible morphological cellular changes within the injured spinal cord in the SCI model were evaluated using H&E staining. At 3 dpi, histological sections showed inflammatory cell infiltration in the SEMA3C group (Figure 2A). Immunostaining of spinal cord sections against iNOS, a marker of M1 microglia,[27] showed that macrophages/microglia took on a proinflammatory phenotype in the core of the lesion after SCI and in the presence of SEMA3C. Immunostaining for inflammation-related indicators RAGE and F4-80 showed similar intensity, which was consistent with western blot analysis (Figures 2B–2F). With the same SCI protocol, immunostaining of fibronectin/MAP2/myelin basic protein (MBP) was used to detect nerve injury with fibronectin staining to outline the lesion, MAP2 labeling to assess neuronal damage and MBP labeling for myelin damage. The results demonstrated that neural damage was more extensive in the presence of SEMA3C (Figures 2G and S1). In addition, protein chip assay showed an increased release of inflammatory cytokines in the SEMA3C treated spinal tissues (Figures 2H–2J).

To determine immune polarization state associated with elevated SEMA3C, we assessed the endogenous transcript and protein levels of SEMA3C in cultured BV2 cells (which are microglial cell lines) after activation with LPS (lipopolysaccharide)/IFN-γ or IL-4/IL-13 (Figures 3A–3C).[28,29] Compared to SEMA3C expressed by control microglia and IL-4/IL-13-induced microglia, the levels of SEMA3C expressed by

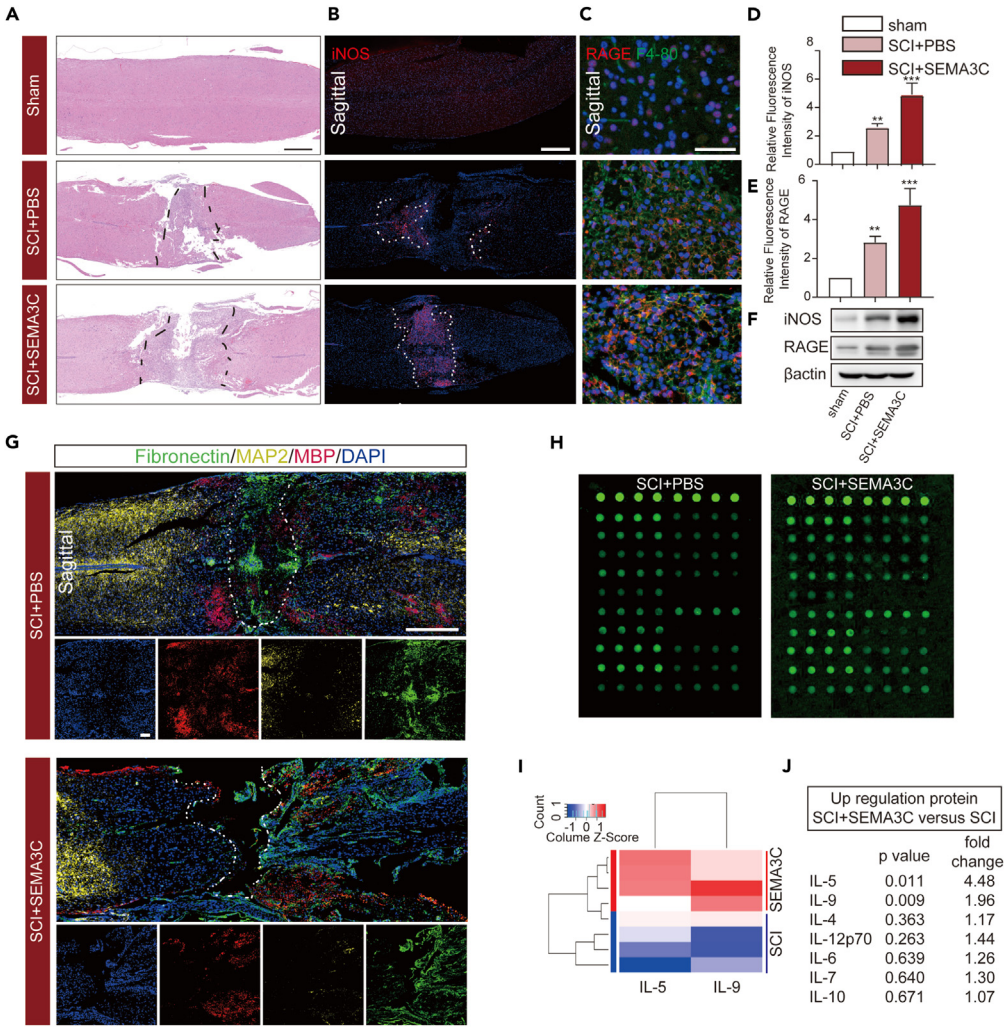

Figure 2. Elevated SEMA3C after experimental SCI in mice aggravates SCI at 3 dpi

(A) Representative low-power magnification image of H&E staining in sagittal spinal cord sections after SCI and injection of either SEMA3C or PBS (control). Neuroinflammation near the lesion core is bounded by dashed lines. Scale bar, 500 μm $n = 3$ per group.

(B) Representative immunofluorescent images of sagittal spinal cord sections after SCI and injection of either SEMA3C or PBS (control) and immunostaining with anti-iNOS antibody (red) to label M1 phenotype microglia. DAPI counterstaining (blue). Dashed white lines indicate boundaries of lesion. $n = 3$ per group. Scale bars, 500 μm (left panel); 100 μm (right panel).

(C) Double immunostaining of microglia for RAGE (red) and F4-80 (green). $n = 3$ per group.

(D and E) Mean (±SD) relative immunofluorescence intensity levels of iNOS (D) and RAGE (E). Significant differences were evaluated by one-way ANOVA and post hoc Dunnett's tests for all panels; *$p < 0.05$; **$p < 0.01$; and ***$p < 0.001$ versus the sham control group ($n = 3$ per group). For iNOS immunofluorescence intensity, $F(2, 6) = 67.89$, R squared = 0.9577, p value <0.0001 in ANOVA summary. For RAGE immunofluorescence intensity, $F(2, 6) = 37.37$, R squared = 0.9257, p value = 0.0004 in ANOVA summary.

(F) Representative western blots of iNOS and RAGE protein (normalized to control protein levels).

(G) Representative immunofluorescent images of sagittal spinal cord sections immunostained for fibronectin (green), MAP2 (yellow), and MBP (red). Sections are from mice after SCI and injection of either SEMA3C or PBS (control). $n = 4$ per group. Dashed white lines indicate boundaries of lesion. Scale bars, 500 μm (upper panel); 200 μm (bottom panel).

(H) Detection of 20 inflammatory cytokines in SCI+PBS-treated mice (control) and SCI+SEMA3C-treated mice using cytokine-antibody array. $n = 4$ per group.

(I) Heatmap showing inflammatory factors ($p < 0.05$) from spinal cord tissue detected by cytokine-antibody array analysis.

(J) Total upregulation of inflammatory cytokines after administration of recombinant SEMA3C to the lesion core after SCI.

LPS/IFN-γ–induced M1 type microglia were considerably elevated. These results suggested that there is increased expression of SEMA3C from M1 type macrophages/microglia, which are also the major macrophage/microglia phenotype present near the lesion core after SCI.[30]

Next, we studied the proinflammatory and pro-apoptotic effects of SEMA3C *in vitro*. BV2 cells were treated with recombinant SEMA3C protein administration. As shown in Figures 3D and 3E, several apoptosis-related proteins were upregulated in SEMA3C-treated BV2 cells.

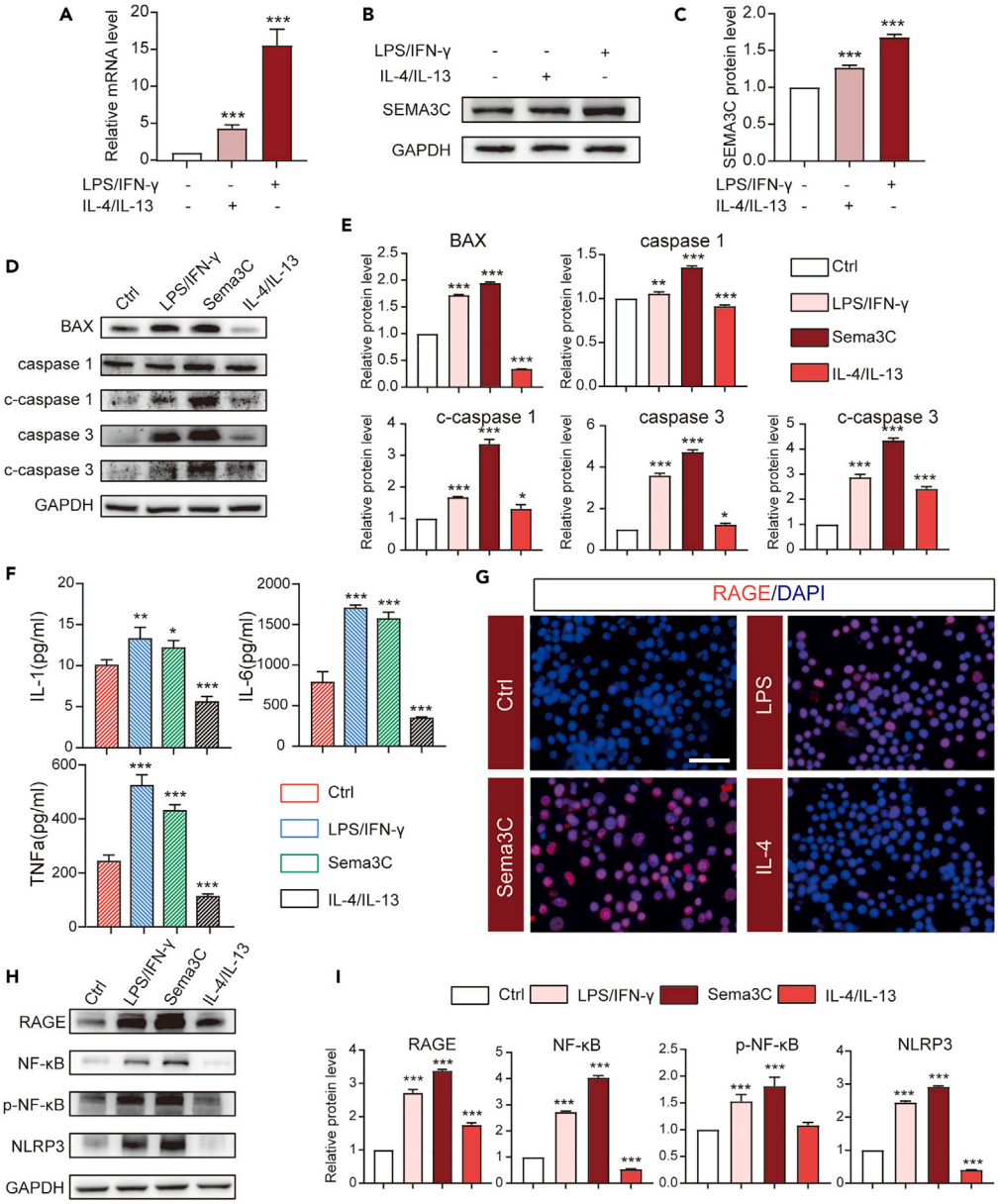

Figure 3. SEMA3C increases neuroinflammation in cultured BV2 microglia

(A) Mean (±SD) relative mRNA expression of SEMA3C, as determined by real-time qPCR, was significantly increased in microglia induced by LPS/IFN-γ to M1 phenotype (n = 11). F (2, 30) = 385.0, R squared = 0.9625, p value <0.0001 in ANOVA summary.

(B and C) Representative western blots and quantitation (normalized to control protein levels, data are represented as mean ± SD) (C) for SEMA3C extracted from cultured BV2 microglia (n = 3). F (2, 6) = 515.4, R squared = 0.9942, p value <0.0001 in ANOVA summary.

(D and E) Relative protein levels and quantitation (mean ± SD) of BAX [F (3, 8) = 18050, R squared = 0.9999, p value <0.0001 in ANOVA summary], caspase −1 [F (3, 8) = 589.0, R squared = 0.9955, p value <0.0001 in ANOVA summary], cleaved caspase 1 [F (3, 8) = 333.0, R squared = 0.9921, p value <0.0001 in ANOVA summary], caspase 3 [F (3, 8) = 1327, R squared = 0.9980, p value <0.0001 in ANOVA summary], and cleaved caspase 3 [F (3, 8) = 756.1, R squared = 0.9965, p value <0.0001 in ANOVA summary] detected by western blot.

(F) Relative (mean ± SD) expression of TNF-α [F (3, 12) = 239.8, R squared = 0.9836, p value <0.0001 in ANOVA summary], IL-6 [F (3, 12) = 313.4, R squared = 0.9874, p value <0.0001 in ANOVA summary], and IL-1β [F (3, 8) = 45.07, R squared = 0.9441, p value <0.0001 in ANOVA summary] in cultured microglia treated with recombinant SEMA3C, as measured by ELISA.

(G) Immunostaining for RAGE (red) in cultured BV2 microglia after LPS or IL-4/IL-13 application. DAPI counterstaining labels nuclei of all cells regardless of activation state. Scale bar, 200μm.

Figure 3. *Continued*

(H and I) Representative western blots and quantitation (mean ± SD) of SEMA3C-activated proteins of the RAGE/NF-κB signaling pathway in cultured microglia. For RAGE analysis, F (3, 8) = 832.0, R squared = 0.9968, *p* value <0.0001 in ANOVA summary. For NF-κB analysis, F (3, 8) = 4198, R squared = 0.9994, *p* value <0.0001 in ANOVA summary. For p-NF-κB analysis, F (3, 8) = 38.14, R squared = 0.9346, *p* value <0.0001 in ANOVA summary. For NLRP3 analysis, F (3, 8) = 5578, R squared = 0.9995, *p* value <0.0001 in ANOVA summary. For all panels with quantitation (A, C, E, F, and I), significant differences were evaluated by one-way ANOVA and post hoc Dunnett's tests; **p* < 0.05; ***p* < 0.01; and ****p* < 0.001 versus untreated control group.

The levels of these proteins were even higher than when LPS/IFN-γ was applied *in vitro* to induce the M1 phenotype of microglia (Figure 3D). We also measured by ELISA several proinflammatory cytokines (TNF-α, IL-6, and IL-1β) in the cell culture media. Cytokine concentration was significantly increased in SEMA3C-treated and LPS/IFN-γ-treated BV2 cells compared to control and IL-4/IL-13-treated cells (Figure 3F). Together, these findings provided evidence that SEMA3C is involved in polarizing microglia to a proinflammatory (M1) and pro-apoptotic state after SCI. They also intriguingly suggest the possibility that secreted SEMA3C influences macrophage/microglia function in an autocrine fashion.

SEMA3C suppresses angiogenesis and antagonizes the effects of recombinant VEGF-A treatment

Blood vessel vascularization and angiogenesis after SCI are critical for nerve repair and recovery.[29] Here, we used human umbilical vein endothelial cells (HUVECs) to determine the role of SEMA3C in regulating angiogenesis *in vitro*. The tube formation assay and scratch-wound assay were replicated and confirmed the important results of Yang et al.[31] In the tube formation assay, SEMA3C-treated HUVECs displayed a meager ability to induce capillary tube formation (Figures 4A and 4B). The angiogenic ability of recombinant vascular endothelial growth factor A (VEGF-A) applied to HUVECs was also partly weakened by SEMA3C pre-treatment.

As angiogenesis is controlled by endothelial cell migration, we next examined whether elevated SEMA3C influenced cell migration. The scratch-wound assay indicated that migration of SEMA3C-treated HUVECs was considerably attenuated compared with that of untreated control or VEGF-A-treated groups (Figures 4C and 4D). We also documented differences in the protein expression of VEGF-A, the master regulator of vascular growth.[32,33] Among the different treatment groups, VEGF-A expression levels were downregulated after SEMA3C treatment (Figure 4E). To further determine the effect, SEMA3C inhibitor (3,5,4′-tribromosalicylanilide) was administrated daily to the lesion core. Specimen was perfused with Microfil and underwent CT analysis using a rat spinal cord injury model to get a more observable perfusion in the rat body size. We found that the vessel diameter and volume increased in the inhibitor-treated SEMA3C group compared to the untreated SCI (control) group (Figures 4F–4H). These results indicated that SEMA3C may have specialized functional properties in suppressing angiogenesis and in antagonizing the angiogenic function of recombinant VEGF-A.

RAGE/NF-κB signaling was activated in SEMA3C-induced pro-inflammatory polarization of microglia

SEMA3C is a secreted glycoprotein that is expressed throughout the lesion core after SCI. Thus, we next aimed to identify the downstream mechanism involved in the neuroinflammation and proinflammatory effects of SEMA3C treatment. After SCI, immunostaining in spinal cord sections near the lesion core for RAGE appeared to be mainly spatially localized within F4-80-positive macrophages/microglia in SEMA3C-treated mice (Figure 2C). This indicates that SEMA3C activated the expression of RAGE.

In *in vitro* experiments with cultured BV2 microglia, we found that RAGE was expressed by SEMA3C-treated microglia, and visually it appeared that most microglia were RAGE-positive (Figure 3G). Western blot analysis revealed that compared to control and IL-4/IL-13-treated groups, SEMA3C treatment upregulated the levels of RAGE, NF-κB p65, phospho-NF-κB p65, and NLRP3 (Figures 3H and 3I), all key factors involved in the RAGE-signaling axis. This suggests that the RAGE/NF-κB signaling pathway may be activated after SCI.

We used molecular docking software to predict the ligand-receptor interaction (Figure 5A). By means of protein-protein interaction analysis in Alphafold and AutoDock software, all functional residues were identified and classified according to their interactions. In the hydrogen bonding interaction, there are multiple groups of residues used to form hydrogen bonds between SEMA3C and RAGE, such as the hydrogen bond formed by His537 of SEMA3C and Arg177 of RAGE (Table S1). With these interaction forces, the scoring for the SEMA3C-RAGE interaction is −562, which is considered good performance.

To confirm the involvement of the RAGE/NF-κB signaling pathway in SEMA3C-induced pro-inflammation and apoptosis in macrophage/microglia, we used FPS-ZM1 in *in vitro* experiments with cultured BV2 cells. FPS-ZM1 is a RAGE-specific inhibitor.[34] Application of FPS-ZM1 considerably decreased the fluorescence intensity, and presumably the number, of iNOS-positive macrophages induced by SEMA3C (Figures 5B and 5C). Inflammation- and apoptosis-related proteins were also effectively downregulated by FPS-ZM1 in SEMA3C-treated cells (Figures 5D and 5E), as was SEMA3C-mediated RAGE signaling molecules (Figures 5F and 5G). Collectively, these results indicated that SEMA3C activated the RAGE/NF-κB signaling pathway neuroinflammation and was involved in the proinflammatory polarization of macrophages/microglia.

Inhibition of SEMA3C-mediated RAGE/NF-κB signaling *in vivo* reduce neuroinflammation and macrophage/microglia polarization after SCI

After acute SCI, proinflammatory macrophages/microglia are recruited to the lesion site, inflammatory cytokines are secreted, including SEMA3C, eventually causing a cascade of secondary injuries to emerge.[35] We hypothesized that in response to SCI, SEMA3C might mediate a pro-immune environment via RAGE/NF-κB signaling.

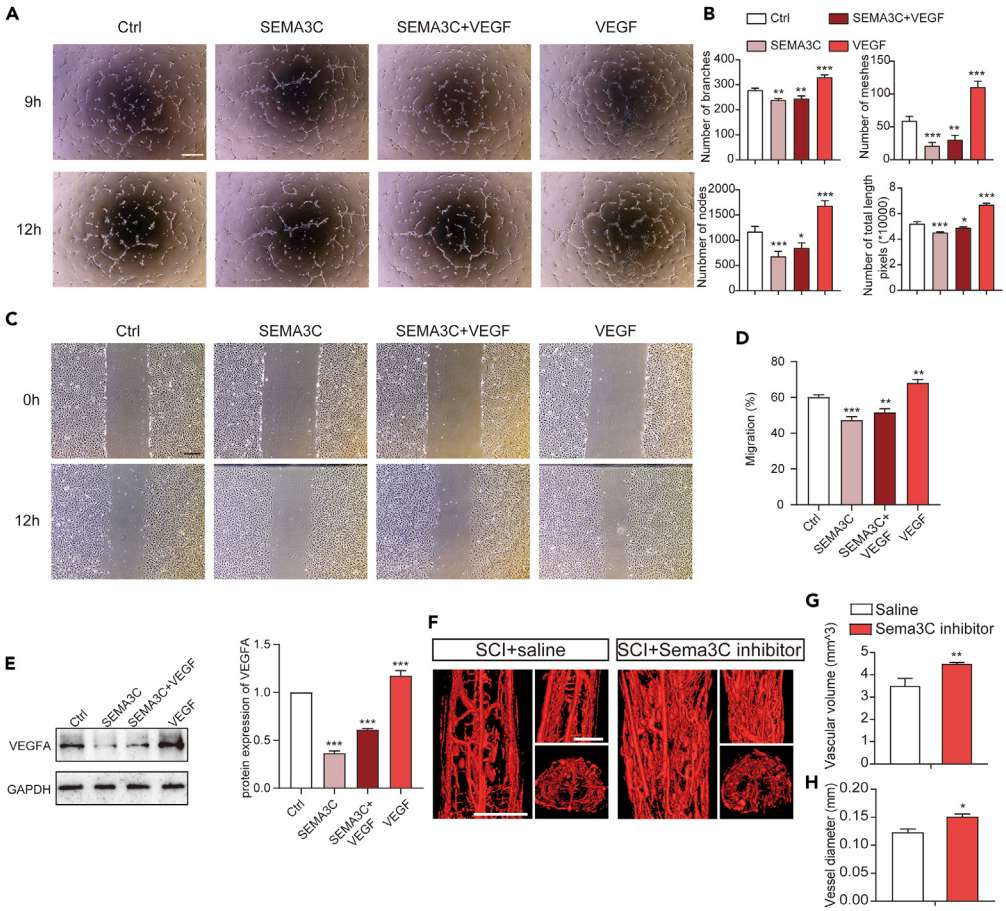

Figure 4. Effects of exogenously applied SEMA3C on human umbilical cord vein endothelial cell (HUVEC) angiogenesis and migration *in vitro*

n = 3 per group.

(A and B) Low-magnification images of capillary-like structures formed by HUVECs (upper) and quantitation (mean ± SD) of the structures as determined by tube-formation assay at the indicated times after application of SEMA3C and/or VEGF-A. Scale bar, 100 μm. For number of branches analysis, F (3, 8) = 66.61, R squared = 0.9615, *p* value <0.0001 in ANOVA summary. For number of meshes analysis, F (3, 8) = 91.39, R squared = 0.9716, *p* value <0.0001 in ANOVA summary. For number of nodes analysis, F (3, 8) = 57.83, R squared = 0.9559, *p* value <0.0001 in ANOVA summary. For number of total length analysis, F (3, 8) = 230.1, R squared = 0.9885, *p* value <0.0001 in ANOVA summary.

(C) Phase-contrast images of SEMA3C-treated HUVECs showing cell migration in scratch-wound assay at the indicated times. Scale bar, 250 μm.

(D) Mean (±SD) rate at which the cell-scratch wound, or gap, "closed" in scratch-wound assay. F (3, 8) = 76.06, R squared = 0.9661, *p* value <0.0001 in ANOVA summary.

(E) Western blots and quantitation (mean ± SD) of VEGF-A protein concentration in HUVECs after exogenous application of SEMA3C. F (3, 8) = 464.9, R squared = 0.9943, *p* value <0.0001 in ANOVA summary.

(F) Representative 3D micro-CT images of the vessel network at 7 dpi. Scale bar, 2 mm.

(G and H) Quantitative analysis (mean ± SD) of the 3D microvasculature in each group. For vascular volume analysis, *p* value = 0.0098, t = 4.630, df = 4. For vessel diameter analysis, *p* value = 0.0211, t = 3.686, df = 4. For all panels with quantitation (B, D, and E), significant differences were evaluated by one-way ANOVA and post hoc Dunnett's tests; for all panels with quantitation (G and H), significant differences were evaluated by Student's t test. *$p < 0.05$; **$p < 0.01$; and ***$p < 0.001$ versus untreated control group.

Next, we tested the hypothesis that inhibiting components of the RAGE pathway might temper or reduce the early inflammatory response driven by SEMA3C, as observed in the microglia response. Iba-1 antibody, which specifically labels microglia,[36] was used to immunostain histological sections after SCI to evaluate regions where macrophages/microglia had infiltrated. FPS-ZM1 treatment showed a lower number of Iba-1 positive cells compared to mice injected with SEMA3C (Figures 6A and 6B).

We further characterized M1/M2 polarization of macrophage/microglia using Arg-1(M2)/CD68 double immunostaining in spinal cord sections after SCI. Pretreatment with FPS-ZM1 resulted in an increase in Arg-1/CD68-positive cells, indicating that SEMA3C-induced proinflammatory polarization was reversed through the inhibition of the RAGE pathway (Figures 6C and 6D). The results were further verified by tissue protein western blot (Figure S2). Additionally, inhibition of the RAGE pathway rapidly decreased SEMA3C immunoreactivity compared with that in the SCI control and in sections from mice receiving local SEMA3C injections. SEMA3C administration also upregulated the expression

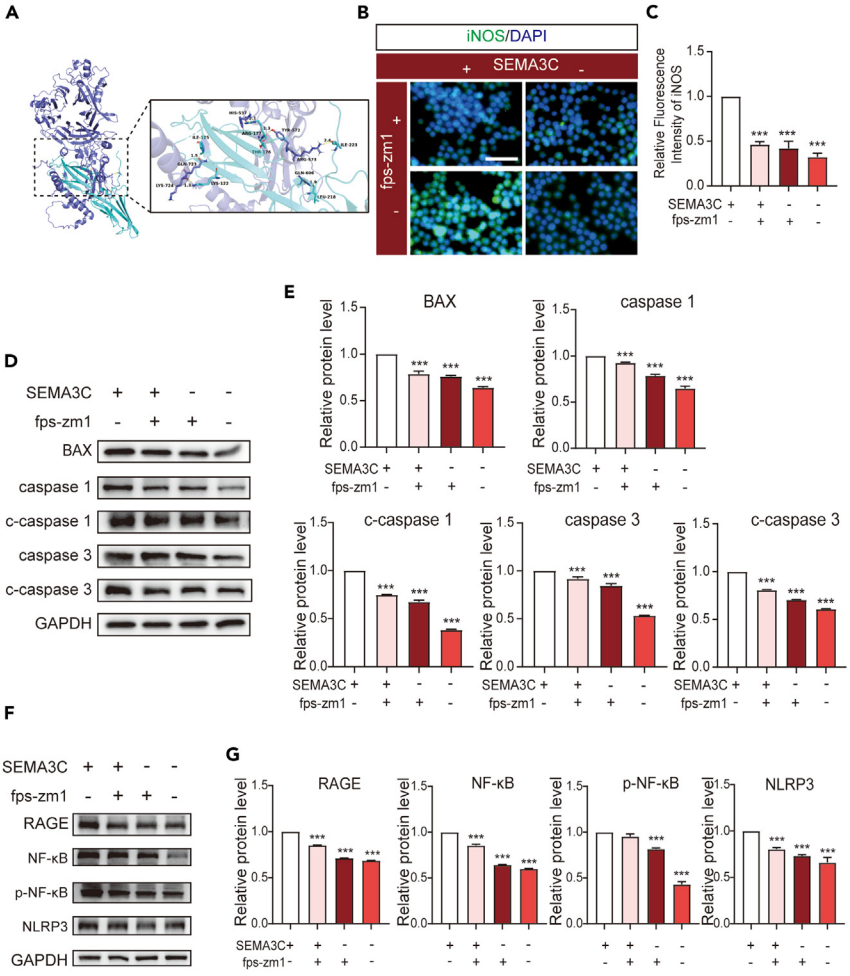

Figure 5. FPS-ZM1 attenuates proinflammatory state and rage/NF-κB signaling pathway activation in SEMA3C-stimulated BV2 cells

n = 3 per group.

(A) Predicted complex structure of SEMA3C-RAGE docking. Complex 3D structure predicted by Alphafold software and AutoDock software. Predicted protein-protein interaction figure was visualized using PyMOL. SEMA3C protein is depicted as a light, purple-colored cartoon-ribbon model, and RAGE protein is depicted as a cyan-colored cartoon model. Ribbons are arranged in PyMOL according to the information in the PDB HELIX and SHEET records. Their binding sites are shown as corresponding-colored stick structures.

(B) Representative epifluorescent images of cultured BV2 cells immunostained for iNOS (green) and counterstained with DAPI after SEMA3C treatment. Scale bar, 200 μm.

(C) Quantitation of mean (±SD) relative intensity of iNOS immunofluorescence for the various groups. F (3, 8) = 123.0, R squared = 0.9788, *p* value <0.0001 in ANOVA summary.

(D and E) Protein levels of BAX [F (3, 8) = 226.1, R squared = 0.9883, *p* value <0.0001 in ANOVA summary], caspase 1 [F (3, 8) = 316.7, R squared = 0.9917, *p* value <0.0001 in ANOVA summary], cleaved caspase 1[F (3, 8) = 1832, R squared = 0.9985, *p* value <0.0001 in ANOVA summary], caspase 3 [F (3, 8) = 534.4, R squared = 0.9950, *p* value <0.0001 in ANOVA summary], and cleaved caspase 3 [F (3, 8) = 3754, R squared = 0.9993, *p* value <0.0001 in ANOVA summary] were measured by western blot and quantitated (mean ± SD) (E) for the same treatment groups and protocol.

(F and G) Protein expression of RAGE [F (3, 8) = 14982, R squared = 0.9998, *p* value <0.0001 in ANOVA summary], NF-κB [F (3, 8) = 2671, R squared = 0.9990, *p* value <0.0001 in ANOVA summary], phospho-NF-κB [F (3, 8) = 487.3, R squared = 0.9946, *p* value <0.0001 in ANOVA summary], and NLRP3 [F (3, 8) = 73.60, R squared = 0.9650, *p* value <0.0001 in ANOVA summary] were measured by western blot and quantitated (mean ± SD) (G). For all panels with quantitation (C, E, and G), significant differences were evaluated by one-way ANOVA and post hoc Dunnett's tests; ***$p < 0.001$ versus the SEMA3C-treated group.

of endogenous SEMA3C, suggesting that feedback might be important in SEMA3C/RAGE signaling (Figures 6E and 6F). These results suggested that after the acute phase after SCI, inhibition of the RAGE/NF-κB signaling pathway effectively reduced neuroinflammation and macrophage/microglia polarization driven by elevated SEMA3C levels.

Inhibition of SEMA3C and the RAGE/NF-κB axis preserve the axons after SCI

Soon after SCI, astrocytes around the injury site become activated and undergo conversion to reactive astrocytes, which proliferate and produce inflammatory cytokines that initially facilitate tissue repair.[37] With time, however, the reactive astrocytes form scar tissue around the lesion core; the

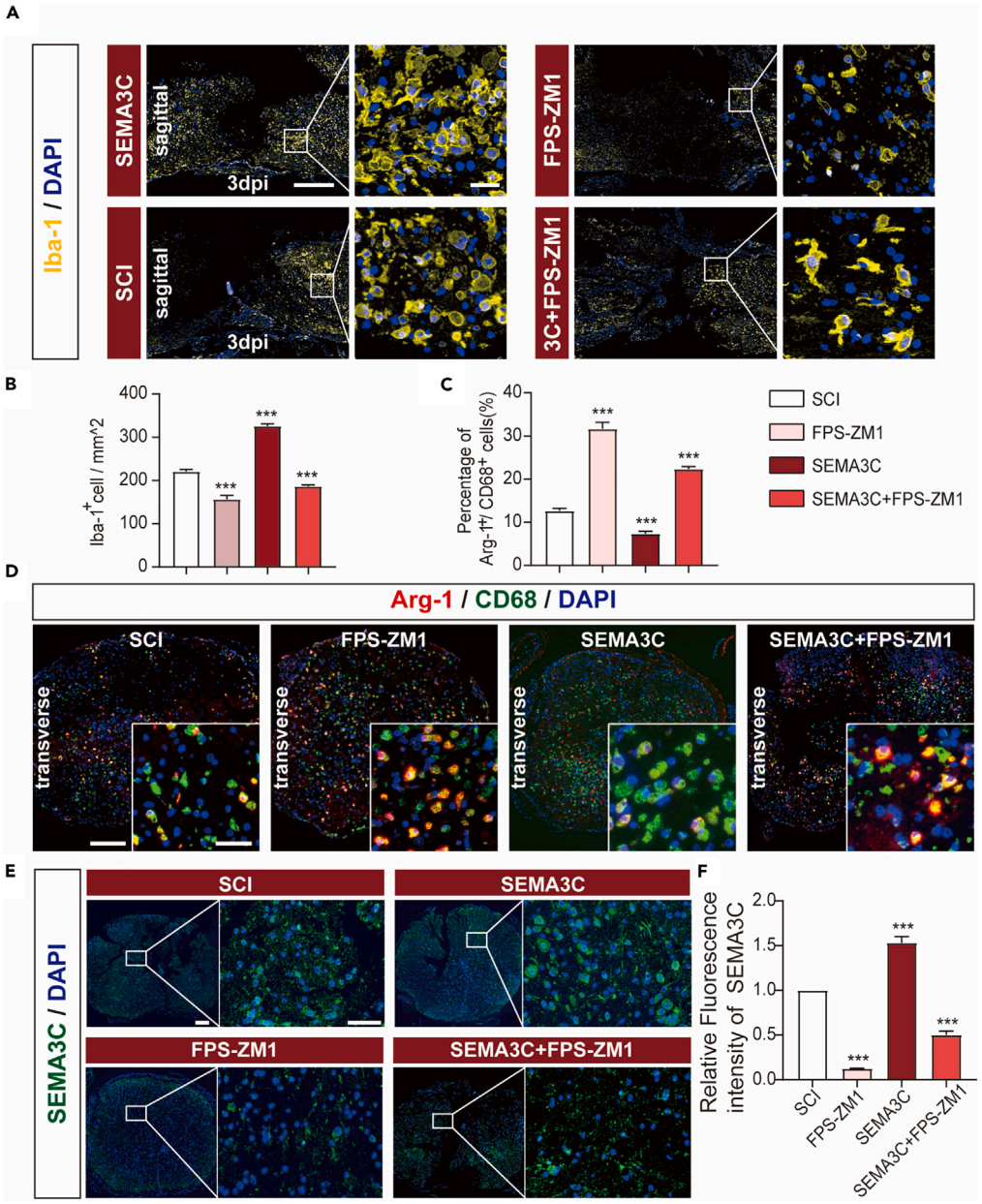

Figure 6. FPS-ZM1 regulates microglia polarization and reduces SEMA3C-mediated neuroinflammation after SCI

3 mice per group.

(A) Representative immunofluorescent images of spinal cord sections 3 days after SCI (3 dpi). The sagittal sections were immunostained for Iba-1 (yellow) and counterstained with DAPI (blue). Low magnification scale bar, 200 μm; high magnification scale bar, 20 μm.

(B and C) Quantitation (mean ± SD) of Iba-1+positive cells (B) and Arg-1/CD68 (C) immunostaining showing mean relative fluorescence normalized to the SCI group. For Iba-1+positive cells analysis, F (3, 8) = 417.9, R squared = 0.9937, *p* value <0.0001 in ANOVA summary. For Arg-1/CD68 (C) immunostaining, F (3, 8) = 416.1, R squared = 0.9936, *p* value <0.0001 in ANOVA summary.

(D) Immunofluorescent images of spinal cord sections at 3 dpi. Sections were immunostained for Arg-1(red)/CD68 (green) and counterstained with DAPI (blue). Scale bars, 200 μm (left panel); 50 μm (right panel).

(E) Immunofluorescent images of spinal cord sections at 3 dpi. Sections are immunostained for SEMA3C (green) and counterstained with DAPI (blue). Scale bars, 200 μm (left panel); 50 μm (right panel).

(F) Quantitation (mean ± SD) of SEMA3C immunostaining showing mean relative fluorescence intensity normalized to the SCI group. F (3, 8) = 662.8, R squared = 0.9960, *p* value <0.0001 in ANOVA summary. For all panels with quantitation (B, C, and F), significant differences were evaluated by one-way ANOVA and post hoc Dunnett's tests; ***$p < 0.001$ versus the SEMA3C-treated group.

extent of this scar tissue determines the severity and prognosis of the injury. Indeed, excessive astrocytic scar formation around the injury site during later stages of SCI is widely regarded to be the principal cause of axonal damage and poor functional outcome.[37] Thus, reactive astrocytosis and associated scar formation have been long considered to be an irreversible aspect of SCI-associated pathology. However, a recent study showed that altering the microenvironment of the lesion site can reverse this process to some extent and even improve tissue repair.[37]

As astrocyte activation is a key indicator of neuronal damage, we wondered whether inhibiting the activation of astrocytes soon after SCI could reduce the formation of reactive astrocytic scars and enhance tissue repair. Thus, we used the RAGE pathway inhibitor FPS-ZM1 and to investigate whether FPS-ZM1 could inhibit SEMA3C-induced astrocytic activation, with the aim of reducing reactive astrocytic scar formation and facilitating repair around the SCI site.

At 1 dpi and 3 dpi in SCI mice treated with FPS-ZM1, we observed fewer GFAP-positive reactive astrocytes than in untreated control SCI mice (Figures 7A and 7B). This pattern of reduced reactive astrocytosis was consistent with the pattern of Iba-1-positive microglia immunostaining during early stages of SCI (Figure 6A). At 28 dpi, SEMA3C induced obvious GFAP-positive astrocytic scar formation around the center of the traumatic spinal lesion (Figure 7C, right panel [top]). However, inhibition of RAGE with FPS-ZM1 markedly decreased astrocytic scar formation (Figure 7C, right panel [bottom]). Immunostaining for GAP43 and double immunostaining for GFAP (astrocyte marker) and Tuj1 (microtubule marker for axons) showed that the FPS-ZM1-associated inhibition of RAGE abolished the inhibitory effect of SEMA3C (Figure 7C). The results were further verified by tissue protein western blot (Figure S2). More microtubules were observed rostral to the lesion core, suggesting axons were preserved from neuroinflammation. These results were further confirmed by serial staining for GAP43, TPH2, and GFAP (Figures 8A and 8B).

Next, to assess neuronal survival after SCI, we counted the number of neurons around the lesion core in Nissl-stained spinal cord sections from SCI mice. Nissl bodies were used as morphological indicators of neuronal survival.[38] We observed significant neuronal loss in the gray matter region of the spinal cord after SCI (*$p < 0.05$ vs. sham group; Figure 7D). At 28 dpi, SCI mice treated with SEMA3C also showed considerable neuronal loss in the spinal cord anterior horn (Figure 7D). However, inhibition of RAGE significantly increased the number of Nissl bodies in SCI mice treated with FPS-ZM1 or SEMA3C+FPS-ZM1 (Figure 7D), suggesting greater neuronal survival. We next performed triple-label immunofluorescence using pgp9.5 (green), NeuN(red), neurofilamment (yellow) on sagittal sections and dual-label IF labeling for NeuN (red) and synaptophysin (green) on transverse sections (Figure 8). The results showed that FPS-ZM1 preserved the axons by suppressing secondary damage by neuroinflammation. In addition, RAGE inhibition treatment stimulated serotonin release (Figure 8C). Transmission electron microscope analysis observed better morphology of myelin sheaths after RAGE inhibition (Figures 8F and 8G). In addition, changes in RAGE protein and inflammation were detected by western blot and immunofluorescence after knockout of Sema3C (Figures 8H and 8I). Taken together, these data indicated that the inhibition of SEMA3C/RAGE preserved axons from neuroinflammation.

DISCUSSION

SEMA3C is among the first axon guidance molecules found to direct axons to appropriate targets. The involvement of semaphorins in immune responses and acute inflammation was reported as early as 2003.[39] Our present study provides the first experimental evidence for SEMA3C being involved in neuroinflammation after SCI and that it may also act in an autocrine manner. We found that SEMA3C is proinflammatory, inducing microglia to polarize toward the M1 phenotype. As the semaphorin family has been implicated in the neuroinflammation associated with secondary pathophysiological processes and injury after SCI, our present findings indicate that SEMA3C may contribute to this refractory stage of SCI. We observed increased expression of SEMA3C after experimentally induced SCI; this increase was sustained for weeks, peaking at 7 dpi and decreasing by 14 dpi. As the temporal profile of SEMA3C expression is consistent with the temporal and spatial profile of microphages/microglia after SCI,[24,25] we hypothesized that the SEMA3C was closely associated with microphages/microglia. Our *in vitro* studies revealed that the M1 phenotype of microglia could express SEMA3C, which acted as an activator of neuroinflammation and subsequent SCI-associated pathology. Mechanistic experiments in the present study revealed that elevated SEMA3C expression led to the activation of the RAGE/NF-κB signaling pathway. Inhibiting SEMA3C-mediated RAGE signaling considerably suppressed production of proinflammatory cytokines, reversed the polarization of the M1 microphage/microglial phenotype, and decreased the number of reactive astrocytes near the lesion core shortly after SCI. Thus, the SEMA3C/RAGE axis appears to be a feasible pathway to target to preserve the axons.

After SCI, the lesion core undergoes complex pathophysiological changes. In contrast to the primary injury caused by direct trauma force onto spinal cord tissue, the secondary injury is the key reason that regeneration and functional nerve recovery is hindered.[40] Generally, secondary injury is divided into acute, subacute, and chronic phases.[41] During the acute phase (within 2–3 days of injury), macrophages/microglia can change their phenotype in response to proinflammatory molecule stimulation; these dominate the local inflammatory response.[42] Persistent exposure to M1 microglia can trigger neuronal dysfunction and promote apoptosis.[43] Although acute inflammation sometimes means protection for the injured organism, amplification of the inflammatory response is an important cause of excessive secondary neuronal injury and poor functional outcomes in SCI.[44] The present study showed that endogenous SEMA3C induced proinflammatory macrophages/microglia and increased expression of apoptosis-related proteins, such as cleaved caspase 3 and BAX.

In the subacute phase (2–14 days after injury), cascade processes underlying reactive astrogliosis, neuronal apoptosis, and axonal degeneration, for example, are at work, resulting in the gradual formation of astrocytic scars. In the chronic phase (2 weeks after injury), astrocytic scars, the ultimate consequence of reactive astrogliosis, becomes firmly established; these scars are reported to be the principal cause of axonal damage and poor functional outcome.[45] Our findings support the idea that astrocytic scars directly impede axonal preservation and that elevated SEMA3C magnifies astrocytic scaring. Therefore, we inhibited SMEA3C-mediated activation of the RAGE pathway after SCI to determine whether astrocytic scaring can be mitigated to some extent that would preserve axons. This inhibition of SMEA3C might further produce axonal elongation.

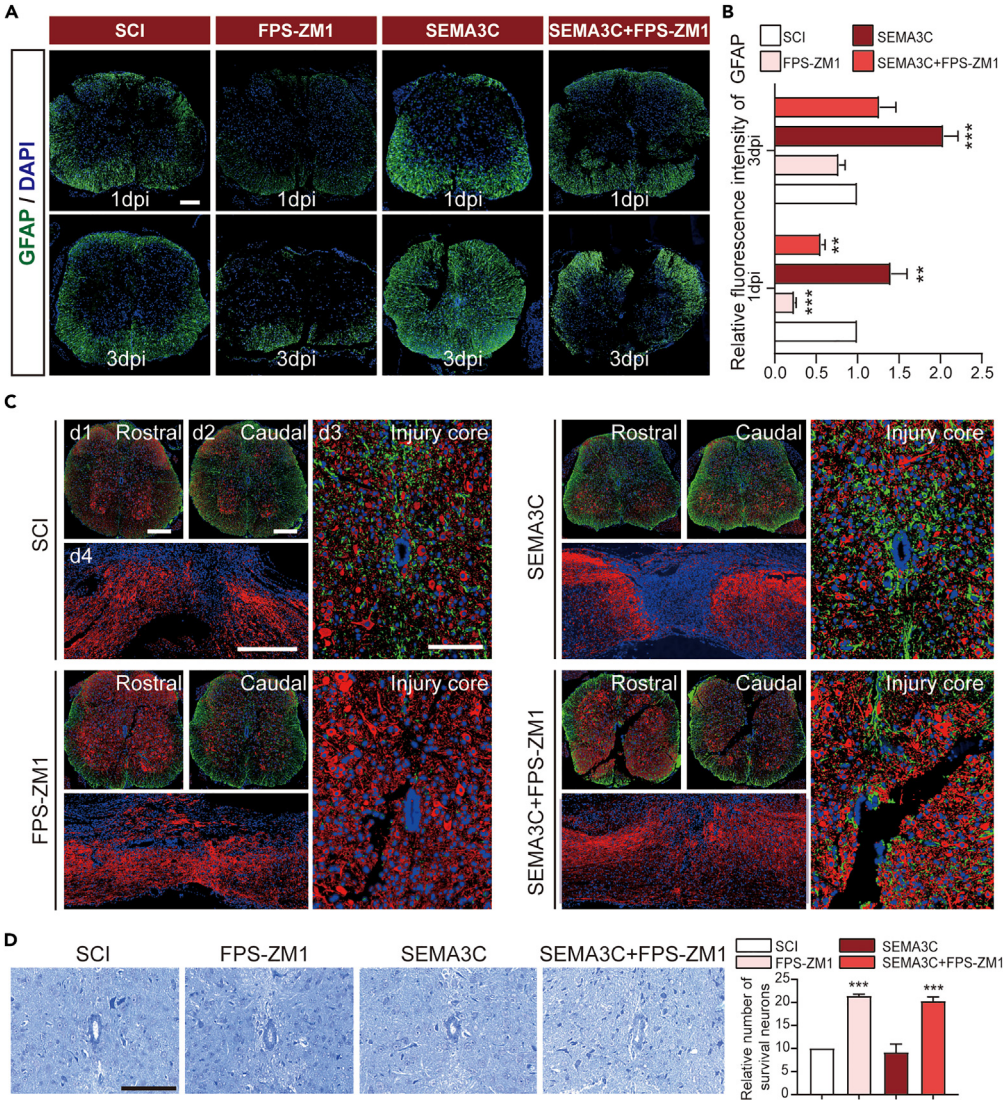

Figure 7. Inhibition of RAGE by FPS-ZM1 improves neuronal survival after SCI

3 mice per group.

(A) Representative immunofluorescent images of A1 astrocytes in spinal cord coronal sections immunostained for the astrocyte marker GFAP at 1 dpi and 3 dpi. Sections are counterstained with DAPI. Scale bar, 200 μm.

(B) Quantitation (mean ± SD) of GFAP immunostaining in spinal cord sections from SCI mice receiving the indicated treatments. Histograms show mean relative fluorescence intensity normalized to that of untreated SCI group. For 1 dpi, F (3, 8) = 49.52, R squared = 0.9489, *p* value <0.0001 in ANOVA summary. For 3 dpi, F (3, 8) = 79.39, R squared = 0.9675, *p* value <0.0001 in ANOVA summary.

(C) Top anatomical schematic shows areas of interest for analysis. Astrocytes and axons of neurons were assessed in spinal cord at 28 dpi. Double immunostaining for GFAP (green) and Tuj1 (red; a microtubule marker in axons) of transverse spinal cord sections at 2 mm intervals; d1, rostral from lesion core; d2, caudal from lesion core; d3, lesion core. Sagittal spinal cord section (d4) immunostained for the axonal marker GAP43 (red). Sections are counterstained with DAPI. Scale bars, 200 μm (d1, d2, d3); 500 μm (d4).

(D) Representative bright-field images of Nissl-stained spinal cord coronal sections at the level of the lesion core at 28 dpi. Histograms (right) show the numbers of Nissl-stained neurons (Nissl bodies) normalized to that of untreated SCI group at 28 dpi (*n* = 3 per group). Data are represented as mean ± SD. F (3, 8) = 120.4, R squared = 0.9783, *p* value <0.0001 in ANOVA summary. For all panels with quantitation (B and D), significant differences were evaluated by one-way ANOVA and post hoc Dunnett's tests; **p* < 0.05, ***p* < 0.01, and ****p* < 0.001 versus SCI group.

One of our primary findings is that SEMA3C may have a previously unreported immunoregulatory function, one relevant for axons preservation after blunt-force trauma. The axons of both the central and peripheral nervous systems are usually guided by growth cones, which sense axon guidance molecules,[46] like semaphorins. The semaphorin family of proteins, which consist of secreted molecules and membrane-spanning proteins, were originally identified to serve as short-range inhibitory molecules that guide growth cones. Recent studies suggest

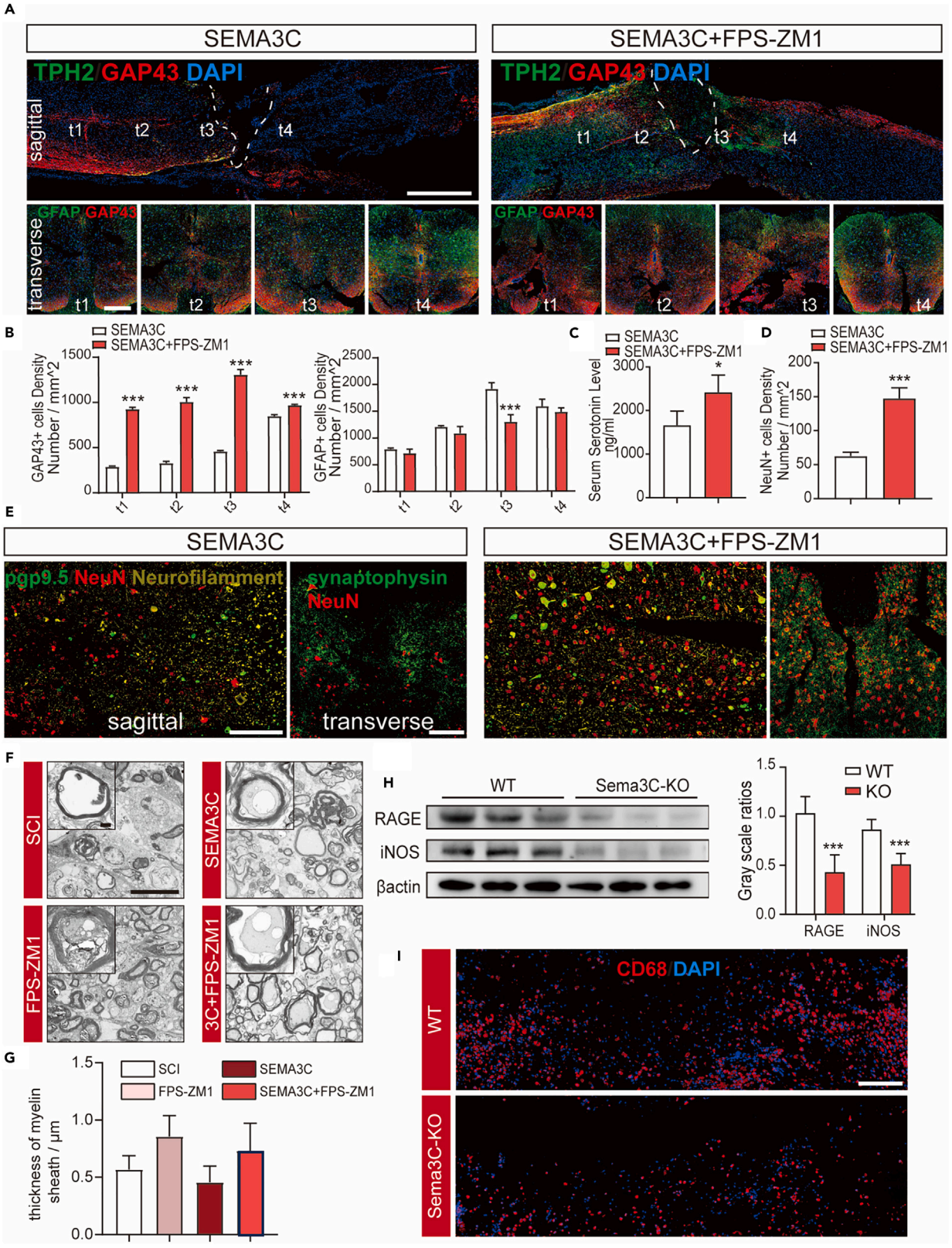
A
SEMA3C
SEMA3C+FPS-ZM1
TPH2 GAP43 DAPI
sagittal
t1
t2
t3
t4
GFAP GAP43
transverse
B
SEMA3C
SEMA3C+FPS-ZM1
GAP43+ cells Density Number / mm^2
GFAP+ cells Density Number / mm^2
C
Serum Serotonin Level ng/ml
D
NeuN+ cells Density Number / mm^2
E
pgp9.5 NeuN Neurofilamment
synaptophysin NeuN
sagittal
transverse
F
SCI
SEMA3C
FPS-ZM1
3C+FPS-ZM1
G
thickness of myelin sheath / μm
H
WT
Sema3C-KO
RAGE
iNOS
βactin
Gray scale ratios
WT
KO
I
CD68 DAPI
WT
Sema3C-KO

Figure 8. FPS-ZM1 improves neuronal survival after SCI

(A) Representative immunofluorescent images for TPH2 (green) and GAP43 (red) in sagittal sections and GFAP (green) and GAP43 (red) in transverse sections 14 dpi. t1–t4 refer to different levels of transverse cardinal plane. The four transverse sections are displayed at interval of 1 mm. Scale bars, 1 mm (upper panel); 200 μm (bottom panel). $n = 3$.

(B) Quantitation (mean ± SD) of GAP43+ and GFAP+ positive cells. Significant differences were evaluated by Student's t test; ***$p < 0.001$ versus the SEMA3C group. In GAP43+ positive cells analysis, For T1, p value < 0.0001, t = 48.49, df = 4. For T2, p value < 0.0001, t = 23.13, df = 4. For T3, p value < 0.0001, t = 24.98, df = 4. For T4, p value = 0.0004, t = 11.23, df = 4. In GFAP+ positive cells analysis, For T1, p value = 0.1633, t = 1.705, df = 4. For T2, p value = 0.1712, t = 1.665, df = 4. For T3, p value = 0.0036, t = 6.122, df = 4. For T4, p value = 0.2879, t = 1.225, df = 4.

(C) Serum serotonin determined by ELISA (mean ± SD). $n = 4$. Significant differences were evaluated by Student's t test; *$p = 0.0253$ versus the SEMA3C group, t = 2.961, df = 6.

(D and E) Representative immunofluorescent images for pgp9.5 (green), NeuN (red), and neurofilamment (yellow) in sagittal sections and synaptophysin (green) and NeuN (red) in transverse sections at 14 dpi. Scale bars, 200 μm. Quantitation of NeuN positive cells (Data are represented as mean ± SD). $n = 3$. Significant differences were evaluated by Student's t test; ***$p = 0.0009$ versus the SEMA3C group. t = 8.753, df = 4.

(F) Transmission electron microscope images of myelin sheath at 14 days after SCI. Scale bar, 100 μm. Small bar insert, 10μm. $n = 5$.

(G) Quantitative analysis (mean ± SD) for diameter of thickness of myelin sheath. Significant differences were evaluated by one-way ANOVA and post hoc Dunnett's tests for all panels. F (3, 16) = 5.365, R squared = 0.5015, p value = 0.0095 in ANOVA summary.

(H) The gray ratio values (mean ± SD) of RAGE (p value = 0.0161, t = 4.004, df = 4) and iNOS (p value = 0.0388, t = 3.029, df = 4) to βactin are shown. WT versus KO mice. $n = 3$. Significant differences were evaluated by Student's t test; *$p < 0.05$ versus the WT group.

(I) Representative immunofluorescent images for CD68 (red) in WT and KO mice. Scale bar, 200 μm.

that certain semaphorins (classes 3, 4, 6, and 7) also play a major role in immune function and bone development.[47] It is well-known that M0 macrophages can be induced to take on the classical proinflammatory M1 phenotype or anti-inflammatory M2 phenotype when exposed to different mediators.[48] For example, Rienks et al. reported that SEMA3A pushed activated M1 macrophages toward a resolution phenotype.[49] On the other hand, SEMA3E was reported to mediate macrophage polarization toward the M1 phenotype.[50] These findings highlight that different classes and subclasses of semaphorins can have varying and opposing effects on immune cells. Moreover, sometimes even one type of semaphorin can produce opposite outcomes in different diseases such as SEMA7A. It was long believed to be a negative mediator of macrophage activation, some researchers found that SEMA7A regulated human macrophages to take on an M2-like phenotype in cases of severe inflammation.[44] This turned our attention back to SEMA3C, which showed proinflammatory properties after SCI in the present study, and also to angiogenesis, which has a close association with neuroinflammation.[51] Our results showed that SEMA3C strongly antagonizes VEGF-A, which may explain previous findings that exogenous addition of VEGF does not significantly stimulate angiogenesis after SCI.[52,53]

We further explored whether SEMA3C might have promise to be used therapeutically after SCI. SEMA3A has been the most studied SEMA3 protein, and as such, antibodies against SEMA3A have already been developed and used to treat mouse sepsis.[54] Therefore, could inhibitors of SEMA3A be used therapeutically to treat other disorders like SCI? One study did indeed observe that SM-216289, a selective inhibitor of SEMA3A, increases regeneration and functional recovery of SCI.[55] We focused on identifying inhibitory molecules downstream of SEMA3C. Our experiments showed that RAGE/NF-κB is activated in response to elevated levels of SEMA3C. Thus, we inhibited SEMA3C signaling via FPS-ZM1, a RAGE-specific inhibitor. FPS-ZM1 inhibited SEMA3C but without the undesirable adverse effects seen in animal models in which Sema3C is knockout.

NF-κB plays important roles in inflammatory diseases, such as rheumatoid arthritis, inflammatory bowel disease, and multiple sclerosis.[56] Proinflammatory cytokines, including IL-1β, IL-6, and TNF-α, are principally encoded by the target genes of the NF-κB p65 canonical pathway.[57] RAGE-mediated signaling was associated with the neuroinflammation found in Alzheimer's disease, along with neuroinflammatory response.[58] Fan et al. recognized that in SCI, the RAGE/NF-κB pathway in M1 macrophages/microglia is activated by damage-associated molecular patterns, molecules released from necrotic cells.[59] Although downstream pathway similarities exist, it is important to recognize that in the CNS semaphorins affect macrophages/microglia function in an autocrine manner. Therefore, the SEMA3C-mediated RAGE/NF-κB pathway may represent a stand-alone mechanism. In addition, the effectiveness of inhibiting the RAGE pathway after SCI could be multifold.

It is widely acknowledged that the neuropilin/plexin (Nrp1/plexin or Nrp2/plexin) co-receptor complex is necessary for class III semaphorins.[60] The present study also observed upregulated expression of Nrp2 *in vivo* after SCI. Although we confirmed that SEMA3C/RAGE signaling occurs after SCI and that Alphafold and Autodock software predicted a reasonable protein-protein interaction model, whether direct protein-protein interaction occurs between SEMA3C and RAGE still requires additional experimental evidence. Moreover, it is unclear how the RAGE-neuropilin complex works. Therefore, the present study can be viewed as a starting point to understanding the involvement of SEMA3C in the immunoregulation of SCI-associated pathophysiological processes. Future research will need to investigate the pattern of how SEMA3C functions in the RAGE pathway and in other cell types after SCI.

In conclusion, we identified a proinflammatory role for SEMA3C in immunoregulation of inflammatory tissue damage after SCI. Our data support the hypothesis that this originally identified nerve repellent factor is likely continuously expressed by macrophages/microglia soon after traumatic SCI, and that elevated SEMA3C expression near the spinal injury activates the RAGE/NF-κB pathway. This cascade of events led to conversion of microglia to the proinflammatory M1 phenotype, reactive astrocytosis, and exacerbated inflammation-associated damage around the lesion core. Inhibiting RAGE effectively preserves the axons by suppressing secondary damage by neuroinflammation and improved behavioral recovery.

Limitations of the study

The present study confirmed an increased expression of SEMA3C in microglia/macrophages, which did not confirm the secretion of SEMA3C from microglia/macrophages.

STAR★METHODS

Detailed methods are provided in the online version of this paper and include the following:

- KEY RESOURCES TABLE
- RESOURCE AVAILABILITY
  - Lead contact
  - Materials availability
  - Data and code availability
- EXPERIMENTAL MODEL AND STUDY PARTICIPANT DETAILS
  - Animals and SCI model for traumatic spinal injury
- METHOD DETAILS
  - Cell culture and treatments
  - Angiogenesis functional assays
  - Micro computed tomography (μCT) scans and analysis
  - Quantitative real-time PCR (real-time qPCR)
  - Western blot analysis
  - Enzyme-linked immunosorbent assay (ELISA)
  - Immunocytochemistry, immunohistochemistry, and histology
  - *In situ* hybridization
  - Cytokine antibody arrays
  - Protein-protein docking analysis
  - Nissl staining
  - Morphological analysis of spinal cord myelin structure
- QUANTIFICATION AND STATISTICAL ANALYSIS
  - Statistical analysis

SUPPLEMENTAL INFORMATION

Supplemental information can be found online at https://doi.org/10.1016/j.isci.2024.109649.

ACKNOWLEDGMENTS

This work was supported by grants from the National Natural Science Foundation of China (NSFC 81974331, 82172421, 82372388, 81930069).

AUTHOR CONTRIBUTIONS

J.S., L.G., and Y.S. wrote the paper. J.S., L.G., J.S., and J.X. performed most of the experiments; J.L., W.H., and J.W. contributed to the morphological study; X.M. and T.G. analyzed the data; Y.C., B.B., Y.Q., and X.Z. designed the research and revised the manuscript. All authors read and approved the final manuscript.

DECLARATION OF INTERESTS

The authors declare that they have no competing interests.

Received: October 12, 2023
Revised: February 1, 2024
Accepted: March 27, 2024
Published: March 29, 2024

REFERENCES

1. Feigin, V.L., Nichols, E., Alam, T., Bannick, M.S., Beghi, E., Blake, N., et al. (2019). Global, regional, and national burden of neurological disorders, 1990–2016: a systematic analysis for the Global Burden of Disease Study 2016. Lancet Neurol. *18*, 459–480.
2. Thuret, S., Moon, L.D.F., and Gage, F.H. (2006). Therapeutic interventions after spinal cord injury. Nat. Rev. Neurosci. *7*, 628–643.
3. Pieczonka, K., and Fehlings, M.G. (2023). Incorporating combinatorial approaches to encourage targeted neural stem/progenitor cell integration following transplantation in spinal cord injury. Stem Cells Transl. Med. *12*, 207–214.
4. Mi, J., Yang, Y., Yao, H., Huan, Z., Xu, C., Ren, Z., Li, W., Tang, Y., Fu, R., and Ge, X. (2021). Inhibition of heat shock protein family A member 8 attenuates spinal cord ischemia-reperfusion injury via astrocyte NF-kappaB/NLRP3 inflammasome pathway. J. Neuroinflammation *18*, 1–12.
5. Paramos-de-Carvalho, D., Martins, I., Cristóvão, A.M., Dias, A.F., Neves-Silva, D., Pereira, T., Chapela, D., Farinho, A., Jacinto, A., and Saúde, L. (2021). Targeting senescent cells improves functional recovery after spinal cord injury. Cell Rep. *36*, 109334.
6. Wang, C., Xu, T., Lachance, B.B., Zhong, X., Shen, G., Xu, T., Tang, C., and Jia, X. (2021). Critical roles of sphingosine kinase 1 in the regulation of neuroinflammation and neuronal injury after spinal cord injury. J. Neuroinflammation *18*, 50.
7. Liddelow, S.A., and Barres, B.A. (2017). Reactive astrocytes: production, function,

and therapeutic potential. Immunity *46*, 957–967.
8. Liu, S., Liu, X., Xiong, H., Wang, W., Liu, Y., Yin, L., Tu, C., Wang, H., Xiang, X., Xu, J., et al. (2019). CXCL13/CXCR5 signaling contributes to diabetes-induced tactile allodynia via activating pERK, pSTAT3, pAKT pathways and pro-inflammatory cytokines production in the spinal cord of male mice. Brain Behav. Immun. *80*, 711–724.
9. David, S., and Kroner, A. (2011). Repertoire of microglial and macrophage responses after spinal cord injury. Nat. Rev. Neurosci. *12*, 388–399.
10. Kolodkin, A.L., Matthes, D.J., and Goodman, C.S. (1993). The semaphorin genes encode a family of transmembrane and secreted growth cone guidance molecules. Cell *75*, 1389–1399.
11. Toledano, S., Nir-Zvi, I., Engelman, R., Kessler, O., and Neufeld, G. (2019). Class-3 semaphorins and their receptors: Potent multifunctional modulators of tumor progression. Int. J. Mol. Sci. *20*, 556.
12. Clark, I.C., Gutiérrez-Vázquez, C., Wheeler, M.A., Li, Z., Rothhammer, V., Linnerbauer, M., Sanmarco, L.M., Guo, L., Blain, M., Zandee, S.E.J., et al. (2021). Barcoded viral tracing of single-cell interactions in central nervous system inflammation. Science *372*, eabf1230.
13. Cai, A., Ye, G., Placier, S., Frère, P., Surin, B., Vandermeersch, S., Kormann, R., Xu-Dubois, Y.C., Genest, M., Lannoy, M., et al. (2022). Genetic inactivation of Semaphorin 3C protects mice from acute kidney injury. Kidney Int. *101*, 720–732.
14. Vieira, J.R., Shah, B., Dupraz, S., Paredes, I., Himmels, P., Schermann, G., Adler, H., Motta, A., Gärtner, L., Navarro-Aragall, A., et al. (2022). Endothelial PlexinD1 signaling instructs spinal cord vascularization and motor neuron development. Neuron *110*, 4074–4089.e6.
15. De Winter, F., Oudega, M., Lankhorst, A.J., Hamers, F.P., Blits, B., Ruitenberg, M.J., Pasterkamp, R.J., Gispen, W.H., and Verhaagen, J. (2002). Injury-induced class 3 semaphorin expression in the rat spinal cord. Exp. Neurol. *175*, 61–75.
16. Ueno, M., Nakamura, Y., Nakagawa, H., Niehaus, J.K., Maezawa, M., Gu, Z., Kumanogoh, A., Takebayashi, H., Lu, Q.R., Takada, M., and Yoshida, Y. (2020). Olig2-Induced Semaphorin Expression Drives Corticospinal Axon Retraction After Spinal Cord Injury. Cerebr. Cortex *30*, 5702–5716.
17. Li, X., Xie, W., Pan, Q., Zhang, X., Zhang, L., Zhao, N., Xie, Q., Ding, J., and Chai, J. (2023). Semaphorin 7A interacts with nuclear factor NF-kappa-B p105 via integrin beta1 and mediates inflammation. Cell Commun. Signal. *21*, 1–16.
18. Adi, S.D., Eiza, N., Bejar, J., Shefer, H., Toledano, S., Kessler, O., Neufeld, G., Toubi, E., and Vadasz, Z. (2019). Semaphorin 3A Is Effective in Reducing Both Inflammation and Angiogenesis in a Mouse Model of Bronchial Asthma. Front. Immunol. *10*, 550.
19. Sakurai, A., Doçi, C.L., and Gutkind, J.S. (2012). Semaphorin signaling in angiogenesis, lymphangiogenesis and cancer. Cell Res. *22*, 23–32.
20. Allen, A.R. (1911). Surgery of experimental lesion of spinal cord equivalent to crush injury of fracture dislocation of spinal column a preliminary report. JAMA *57*, 878–880.
21. Cheriyan, T., Ryan, D.J., Weinreb, J.H., Cheriyan, J., Paul, J.C., Lafage, V., Kirsch, T., and Errico, T.J. (2014). Spinal cord injury models: a review. Spinal Cord *52*, 588–595.
22. Sidhu, G.S., Ghag, A., Prokuski, V., Vaccaro, A.R., and Radcliff, K.E. (2013). Civilian gunshot injuries of the spinal cord: a systematic review of the current literature. Clin. Orthop. Relat. Res. *471*, 3945–3955.
23. Courtine, G., Bunge, M.B., Fawcett, J.W., Grossman, R.G., Kaas, J.H., Lemon, R., Maier, I., Martin, J., Nudo, R.J., Ramon-Cueto, A., et al. (2007). Can experiments in nonhuman primates expedite the translation of treatments for spinal cord injury in humans? Nat. Med. *13*, 561–566.
24. Li, C., Wu, Z., Zhou, L., Shao, J., Hu, X., Xu, W., Ren, Y., Zhu, X., Ge, W., Zhang, K., et al. (2022). Temporal and spatial cellular and molecular pathological alterations with single-cell resolution in the adult spinal cord after injury. Signal Transduct. Targeted Ther. *7*, 65.
25. Milich, L.M., Choi, J.S., Ryan, C., Cerqueira, S.R., Benavides, S., Yahn, S.L., Tsoulfas, P., and Lee, J.K. (2021). Single-cell analysis of the cellular heterogeneity and interactions in the injured mouse spinal cord. J. Exp. Med. *218*, e20210040.
26. Austyn, J.M., and Gordon, S. (1981). F4/80, a monoclonal antibody directed specifically against the mouse macrophage. Eur. J. Immunol. *11*, 805–815.
27. Xia, W., Zou, C., Chen, H., Xie, C., and Hou, M. (2020). Immune checkpoint inhibitor induces cardiac injury through polarizing macrophages via modulating microRNA-34a/Kruppel-like factor 4 signaling. Cell Death Dis. *11*, 575.
28. Cho, D.I., Kim, M.R., Jeong, H.Y., Jeong, H.C., Jeong, M.H., Yoon, S.H., Kim, Y.S., and Ahn, Y. (2014). Mesenchymal stem cells reciprocally regulate the M1/M2 balance in mouse bone marrow-derived macrophages. Exp. Mol. Med. *46*, e70.
29. Huang, T., Shen, J., Bao, B., Hu, W., Sun, Y., Zhu, T., Lin, J., Gao, T., Li, X., and Zheng, X. (2022). Mitochondrial-targeting antioxidant MitoQ modulates angiogenesis and promotes functional recovery after spinal cord injury. Brain Res. *1786*, 147902.
30. Kigerl, K.A., Gensel, J.C., Ankeny, D.P., Alexander, J.K., Donnelly, D.J., and Popovich, P.G. (2009). Identification of two distinct macrophage subsets with divergent effects causing either neurotoxicity or regeneration in the injured mouse spinal cord. J. Neurosci. *29*, 13435–13444.
31. Yang, W.J., Hu, J., Uemura, A., Tetzlaff, F., Augustin, H.G., and Fischer, A. (2015). Semaphorin-3C signals through Neuropilin-1 and PlexinD1 receptors to inhibit pathological angiogenesis. EMBO Mol. Med. *7*, 1267–1284.
32. Nieves, B.J., D'Amore, P.A., and Bryan, B.A. (2009). The function of vascular endothelial growth factor. Biofactors *35*, 332–337.
33. Zhang, D., Lindstrom, A., Kim, E.J., Hwang, C.I., Hall, M.L., Lin, T.Y., and Li, Y. (2022). SEMA3C Supports Pancreatic Cancer Progression by Regulating the Autophagy Process and Tumor Immune Microenvironment. Front. Oncol. *12*, 890154.
34. Deane, R., Singh, I., Sagare, A.P., Bell, R.D., Ross, N.T., LaRue, B., Love, R., Perry, S., Paquette, N., Deane, R.J., et al. (2012). A multimodal RAGE-specific inhibitor reduces amyloid beta-mediated brain disorder in a mouse model of Alzheimer disease. J. Clin. Invest. *122*, 1377–1392.
35. Hellenbrand, D.J., Quinn, C.M., Piper, Z.J., Morehouse, C.N., Fixel, J.A., and Hanna, A.S. (2021). Inflammation after spinal cord injury: a review of the critical timeline of signaling cues and cellular infiltration. J. Neuroinflammation *18*, 284.
36. Ito, D., Imai, Y., Ohsawa, K., Nakajima, K., Fukuuchi, Y., and Kohsaka, S. (1998). Microglia-specific localisation of a novel calcium binding protein. Brain Res. Mol. Brain Res. *57*, 1–9.
37. Hara, M., Kobayakawa, K., Ohkawa, Y., Kumamaru, H., Yokota, K., Saito, T., Kijima, K., Yoshizaki, S., Harimaya, K., Nakashima, Y., and Okada, S. (2017). Interaction of reactive astrocytes with type I collagen induces astrocytic scar formation through the integrin-N-cadherin pathway after spinal cord injury. Nat. Med. *23*, 818–828.
38. Luo, Q., Lin, Y.X., Yang, P.P., Wang, Y., Qi, G.B., Qiao, Z.Y., Li, B.N., Zhang, K., Zhang, J.P., Wang, L., and Wang, H. (2018). A self-destructive nanosweeper that captures and clears amyloid beta-peptides. Nat. Commun. *9*, 1802.
39. Kumanogoh, A., and Kikutani, H. (2003). Roles of the semaphorin family in immune regulation. Adv. Immunol. *81*, 173–198.
40. Chen, S., Ye, J., Chen, X., Shi, J., Wu, W., Lin, W., Lin, W., Li, Y., Fu, H., and Li, S. (2018). Valproic acid attenuates traumatic spinal cord injury-induced inflammation via STAT1 and NF-kappaB pathway dependent of HDAC3. J. Neuroinflammation *15*, 1–14.
41. David, G., Mohammadi, S., Martin, A.R., Cohen-Adad, J., Weiskopf, N., Thompson, A., and Freund, P. (2019). Traumatic and nontraumatic spinal cord injury: pathological insights from neuroimaging. Nat. Rev. Neurol. *15*, 718–731.
42. Van Broeckhoven, J., Sommer, D., Dooley, D., Hendrix, S., and Franssen, A.J.P.M. (2021). Macrophage phagocytosis after spinal cord injury: when friends become foes. Brain *144*, 2933–2945.
43. Kong, X., and Gao, J. (2017). Macrophage polarization: a key event in the secondary phase of acute spinal cord injury. J. Cell Mol. Med. *21*, 941–954.
44. Körner, A., Bernard, A., Fitzgerald, J.C., Alarcon-Barrera, J.C., Kostidis, S., Kaussen, T., Giera, M., and Mirakaj, V. (2021). Sema7A is crucial for resolution of severe inflammation. Proc. Natl. Acad. Sci. USA *118*, e2017527118.
45. Cregg, J.M., DePaul, M.A., Filous, A.R., Lang, B.T., Tran, A., and Silver, J. (2014). Functional regeneration beyond the glial scar. Exp. Neurol. *253*, 197–207.
46. Chilton, J.K. (2006). Molecular mechanisms of axon guidance. Dev. Biol. *292*, 13–24.
47. Rosenberger, C. (2022). Semaphorin class 3C, vascular permeability, and the swollen injured kidney. Kidney Int. *101*, 670–673.
48. Locati, M., Mantovani, A., and Sica, A. (2013). Macrophage activation and polarization as an adaptive component of innate immunity. Adv. Immunol. *120*, 163–184.
49. Rienks, M., Carai, P., Bitsch, N., Schellings, M., Vanhaverbeke, M., Verjans, J., Cuijpers, I., Heymans, S., and Papageorgiou, A. (2017). Sema3A promotes the resolution of cardiac inflammation after myocardial infarction. Basic Res. Cardiol. *112*, 42.
50. Mohammed, A., Okwor, I., Shan, L., Onyilagha, C., Uzonna, J.E., and Gounni, A.S. (2020). Semaphorin 3E Regulates the Response of Macrophages to

Lipopolysaccharide-Induced Systemic Inflammation. J. Immunol. *204*, 128–136.
51. Edlmann, E., Giorgi-Col, L.S., Whitfield, P.C., Carpenter, K.L.H., and Hutchinson, P.J. (2017). Pathophysiology of chronic subdural haematoma: inflammation, angiogenesis and implications for pharmacotherapy. J. Neuroinflammation *14*, 1–13.
52. Benton, R.L., and Whittemore, S.R. (2003). VEGF165 therapy exacerbates secondary damage following spinal cord injury. Neurochem. Res. *28*, 1693–1703.
53. Benton, R.L., Maddie, M.A., Gruenthal, M.J., Hagg, T., and Whittemore, S.R. (2009). Neutralizing endogenous VEGF following traumatic spinal cord injury modulates microvascular plasticity but not tissue sparing or functional recovery. Curr. Neurovascular Res. *6*, 124–131.
54. Yamashita, N., Jitsuki-Takahashi, A., Ogawara, M., Ohkubo, W., Araki, T., Hotta, C., Tamura, T., Hashimoto, S.I., Yabuki, T., Tsuji, T., et al. (2015). Anti-Semaphorin 3A neutralization monoclonal antibody prevents sepsis development in lipopolysaccharide-treated mice. Int. Immunol. *27*, 459–466.
55. Kaneko, S., Iwanami, A., Nakamura, M., Kishino, A., Kikuchi, K., Shibata, S., Okano, H.J., Ikegami, T., Moriya, A., Konishi, O., et al. (2006). A selective Sema3A inhibitor enhances regenerative responses and functional recovery of the injured spinal cord. Nat. Med. *12*, 1380–1389.
56. Li, Q., and Verma, I.M. (2002). NF-kappaB regulation in the immune system. Nat. Rev. Immunol. *2*, 725–734.
57. Karin, M., and Greten, F.R. (2005). NF-kappaB: linking inflammation and immunity to cancer development and progression. Nat. Rev. Immunol. *5*, 749–759.
58. Deane, R., Singh, I., Sagare, A.P., Bell, R.D., Ross, N.T., LaRue, B., Love, R., Perry, S., Paquette, N., Deane, R.J., et al. (2012). A multimodal RAGE-specific inhibitor reduces amyloid β-mediated brain disorder in a mouse model of Alzheimer disease. J. Clin. Invest. *4*, 1377–1392.
59. Fan, H., Tang, H.B., Chen, Z., Wang, H.Q., Zhang, L., Jiang, Y., Li, T., Yang, C.F., Wang, X.Y., Li, X., et al. (2020). Inhibiting HMGB1-RAGE axis prevents pro-inflammatory macrophages/microglia polarization and affords neuroprotection after spinal cord injury. J. Neuroinflammation *17*, 295.
60. Takahashi, T., Nakamura, F., Jin, Z., Kalb, R.G., and Strittmatter, S.M. (1998). Semaphorins A and E act as antagonists of neuropilin-1 and agonists of neuropilin-2 receptors. Nat. Neurosci. *1*, 487–493.
61. Schneider, C.A., Rasband, W.S., and Eliceiri, K.W. (2012). NIH Image to ImageJ: 25 years of image analysis. Nat. Methods *9*, 671–675.
62. Carpentier, G., Berndt, S., Ferratge, S., Rasband, W., Cuendet, M., Uzan, G., and Albanese, P. (2020). Angiogenesis analyzer for ImageJ—A comparative morphometric analysis of "endothelial tube formation assay" and "fibrin bead assay". Sci. Rep. *10*, 11568.
63. Morris, G.M., Huey, R., and Olson, A.J. (2008). Using AutoDock for ligand-receptor docking. Curr. Protoc. Bioinformatics *Chapter 8*. Unit 8.14.
64. Hu, J., Yang, Z., Li, X., and Lu, H. (2016). CC motif chemokine ligand 20 regulates neuroinflammation following spinal cord injury via Th17 cell recruitment. J. Neuroinflammation *13*, 162.
65. Kashiwagi, T., Takazawa, Y., Kagawa, T., and Taga, T. (2023). Organization of self-advantageous niche by neural stem/progenitor cells during development via autocrine VEGF-A under hypoxia. Inflamm. Regen. *43*, 8–15.
66. Stamm, A., Reimers, K., Strauß, S., Vogt, P., Scheper, T., and Pepelanova, I. (2016). *In vitro* wound healing assays–state of the art. BioNanoMaterials *17*, 79–87.
67. Lee, C.C.W., Munuganti, R.S.N., Peacock, J.W., Dalal, K., Jiao, I.Z.F., Shepherd, A., Liu, L., Tam, K.J., Sedgwick, C.G., Bhasin, S., et al. (2018). Targeting semaphorin 3C in prostate cancer with small molecules. J. Endocr. Soc. *2*, 1381–1394.
68. Zhang, D., Lindstrom, A., Kim, E.J., Hwang, C.I., Hall, M.L., Lin, T.Y., and Li, Y. (2022). SEMA3C supports pancreatic cancer progression by regulating the autophagy process and tumor immune microenvironment. Front. Oncol. *12*, 890154.
69. Lee, S., Barbe, M.F., Scalia, R., and Goldfinger, L.E. (2014). Three-dimensional reconstruction of neovasculature in solid tumors and basement membrane matrix using ex vivo X-ray microcomputed tomography. Microcirculation *21*, 159–170.
70. Bryant, P., Pozzati, G., and Elofsson, A. (2022). Improved prediction of protein-protein interactions using AlphaFold2. Nat. Commun. *13*, 1265.
71. Jumper, J., Evans, R., Pritzel, A., Green, T., Figurnov, M., Ronneberger, O., Tunyasuvunakool, K., Bates, R., Žídek, A., Potapenko, A., et al. (2021). Highly accurate protein structure prediction with AlphaFold. Nature *596*, 583–589.
72. Katchalski-Katzir, E., Shariv, I., Eisenstein, M., Friesem, A.A., Aflalo, C., and Vakser, I.A. (1992). Molecular surface recognition: determination of geometric fit between proteins and their ligands by correlation techniques. Proc. Natl. Acad. Sci. USA *89*, 2195–2199.
73. Vakser, I.A. (1996). Long-distance potentials: an approach to the multiple-minima problem in ligand-receptor interaction. Protein Eng. *9*, 37–41.

STAR★METHODS

KEY RESOURCES TABLE

REAGENT or RESOURCE	SOURCE	IDENTIFIER
Antibodies		
Rabbit polyclonal anti-mouse/human SEMA3C	Invitrogen, ThermoFisher	Cat# PA5-90429; RRID: AB_2806070
Rabbit monoclonal anti-mouse/rat BAX (D3R2M)	Cell Signaling Technology	Cat# 14796; RRID: AB_2716251
Rabbit polyclonal anti-mouse caspase 1	Abcam	Cat# ab138483; RRID: AB_2888675
Rat monoclonal anti-mouse/rat c caspase 1	Abclonal	Cat# A21085; RRID: AB_3065496
Rabbit monoclonal anti-mouse/rat/human caspase 3	Abcam	Cat# ab184787; RRID: AB_2827742
Rabbit monoclonal anti-mouse c caspase 3	Abcam	Cat# ab214430; RRID: AB_2938798
Rabbit monoclonal anti-mouse/rat/human RAGE	Abcam	Cat# ab216329; RRID: AB_2884897
Rabbit monoclonal anti-mouse/rat/human/ hamster/monkey/dog NF-κB p65	Cell Signaling Technology	Cat# 8242; RRID: AB_10859369
Rabbit monoclonal anti- mouse/rat/huma/monkey/ pig phospho NF-κB p65	Cell Signaling Technology	Cat# 3033; RRID: AB_331284
Rabbit monoclonal anti-mouse/human NLRP3	Cell Signaling Technology	Cat# 15101; RRID: AB_2722591
Rabbit monoclonal anti-mouse/rat/human VEGFA	Abcam	Cat# ab214424; RRID:;AB_ 3064726
Rabbit monoclonal mouse/rat/human anti-Arg-1	Abclonal	Cat# A4923; RRID: AB_2863390
Rabbit monoclonal anti-mouse/rat/human Iba-1	Abcam	Cat# Ab178846; RRID: AB_2636859
Rabbit monoclonal anti-mouse/human iNOS	Abclonal	Cat# A3774; RRID: AB_3094627
Mouse monoclonal anti-mouse/rat/human/ common marmosetTuj1	Abcam	Cat# Ab78078; RRID:AB_2256751
Rabbit monoclonal anti-mouse/rat/ human/monkey GAPDH	Cell Signaling Technology	Cat# 5174; RRID: AB_10622025
Mouse monoclonal anti-mouse/rat/human beta actin	Abcam	Cat# Ab8226; RRID:AB_306371
Rabbit polyclonal anti-mouse/human SEMA3C	Invitrogen, ThermoFisher	Cat# PA5-90429; RRID: AB_2806070
Rat monoclonal anti-mouse F4-80	Abcam	Cat# ab6640; RRID: AB_1140040
Rabbit monoclonal anti-mouse/rat/human iNOS	Abcam	Cat# ab178945; RRID: AB_2861417
Rabbit monoclonal anti-mouse/rat/human RAGE	Abcam	Cat# ab216329; RRID: AB_2884897
Rabbit monoclonal anti-mouse/rat/human Iba-1	Abcam	Cat# ab178846; RRID: AB_2636859

(*Continued on next page*)

Continued

REAGENT or RESOURCE	SOURCE	IDENTIFIER
Rabbit monoclonal anti-mouse/rat/human Arginase-1	Cell Signaling Technology	Cat# 93668; RRID: AB_2800207
Rabbit monoclonal anti-mouse/rat/hamster CD68	Cell Signaling Technology	Cat# 97778; RRID: AB_2928056
Rabbit polyclonal anti-mouse/rat GFAP	Abcam	Cat# ab7260; RRID: AB_305808
Rabbit polyclonal anti-mouse/rat/human/common marmoset Tuj1	Abcam	Cat# ab18207; RRID: AB_444319
Mouse monoclonal anti-mouse/rat/human GAP43	Abcam	Cat# ab75810; RRID: AB_1310252
Rabbit monoclonal anti-mouse/rat/human TPH2	Cell Signaling Technology	Cat# 51124; RRID: AB_2799385
Rabbit monoclonal anti-mouse/rat/human fibronectin	Abcam	Cat# ab268020; RRID: AB_2941028
Rabbit polyclonal anti-mouse/rat/human MAP2	Merck Millipore/Sigma-Aldrich	Cat# AB5622; RRID: AB_91939
Rabbit monoclonal anti-mouse/rat/human Myelin basic protein (MBP)	Cell Signaling Technology	Cat# 78896; RRID: AB_2799920
Rabbit monoclonal anti-mouse/rat/human NeuN	Cell Signaling Technology	Cat# 24307; RRID: AB_2651140
Rabbit monoclonal anti-mouse/rat/ human synaptophysin	Cell Signaling Technology	Cat# 36406; RRID: AB_2799098
Mouse monoclonal anti-mouse/rat/ human neurofilament-H	Cell Signaling Technology	Cat# 2836; RRID:AB_10694081
Mouse monoclonal anti-mouse/rat/ human/monkey pgp9.5 (ubiquitin C-terminal hydrolase L1 [UCHL1])	Cell Signaling Technology	Cat# 60702; RRID: None
Goat Anti-Mouse IgG HRP	Jackson ImmunoResearch	#115-035-003; RRID: AB_10015289
Goat Anti-Rabbit IgG HRP	Jackson ImmunoResearch	#111-035-003; RRID: AB_2313567
Goat Anti-Rat IgG HRP	Cell Signaling Technology	Cat# 7077; RRID:AB_10694715
Goat Anti-Rabbit IgG H&L (Alexa Fluor® 488)	Abcam	Cat# ab150077; RRID:AB_2630356
Goat Anti-Mouse IgG H&L (Alexa Fluor® 488)	Abcam	Cat# ab150113; RRID:AB_2576208
Goat Anti-Rabbit IgG H&L (Alexa Fluor® 594)	Abcam	Cat# ab150080; RRID:AB_2650602
Goat Anti-Mouse IgG H&L (Alexa Fluor® 594)	Abcam	Cat# ab150116; RRID:AB_2650601
Chemicals, peptides, and recombinant proteins		
Recombinant SEMA3C	R&D Systems	Cat# 1728-S3
FPS-ZM1	MedChemExpress	Cat# HY-19370
Escherichia coli (O55:B5) lipopolysaccharide	Sigma	Cat# L2880
Recombinant murine IFN-γ	Peprotech	Cat# 315-05
IL-4	R&D Systems	Cat# P07750
IL-13	R&D Systems	Cat# P20109

(*Continued on next page*)

Continued

REAGENT or RESOURCE	SOURCE	IDENTIFIER
recombinant VEGF-A	R&D Systems	Cat# 493-MV-025/CF
3,5,4′-tribromosalicylanilide	TCI Chemicals	Cat# T0356; CAS: 87-10-5
Critical commercial assays		
EZ-press RNA Purification Kit	EZBioscience	Cat# B0004D-100
cDNA Reverse Transcription Kit	EZBioscience	Cat# RT3/RT3-L
SYBR Green I Master Mix	EZBioscience	Cat# CQ20
BCA protein assay kit	Cell Signaling Technology	Cat# 7780
TNF-α ELISA Kit	Anogen	Cat# MEC1003
IL-6 ELISA Kit	Anogen	Cat# MEC1008
IL-1β ELISA Kit	Anogen	Cat# MEC1010
ELISA kit specific for serum serotonin	Labor Diagnostika Nord Gmbh & Co.KG	Cat# BA E-8900
Multiplexed Quantibody® Mouse Interleukin Array	RayBiotech, Inc.	Cat# QAM-INT-1
Deposited data		
General data	Zenodo	https://doi.org/10.5281/zenodo.10866254
Experimental models: Cell lines		
Murine microglial BV2 cells	Zhong Qiao Xin Zhou Biotechnology Co., Ltd.	Cat# ZQ0397
Human umbilical vein endothelial cells (HUVECs)	ScienCell Research Laboratories, Inc.	Cat# 8000
Experimental models: Organisms/strains		
Sema3c Cas-9-KO	GemPharmatech™ Co., Ltd.	Strain No.T035361
C57BL/6J mice	Shanghai Sixth People's Hospital vivarium	N/A
Sprague-Dawley rats	Shanghai Sixth People's Hospital vivarium	N/A
Oligonucleotides		
Mouse SEMA3C primers for RT-PCR F: 5′ GTGTGATGCTAACACCATCCT3 3′ R: 5′ CTGGCAGTTTGAAGGTAAGTG 3′	This paper	N/A
Mouse NRP2 primers for RT-PCR F: 5′ ACAGTTCCTGACCTTTGACCT 3′ R: 5′ CAGATGTCCAGCCAGTCATAT 3′	This paper	N/A
Mouse GAPDH primers for RT-PCR F: 5′ AAATGGTGAAGGTCGGTGTG 3′ R: 5′ AGGTCAATGAAGGGGTCGTT 3′	This paper	N/A
Sema3C genotyping primers F1: 5′-GCATACACACATTTAATGTTGCCTG-3′ R1: 5′-CAGTGAGAGTAAGTCATGCACAGAGATC-3′ F2: 5′-CTGGTTCGGATAAAGGAAGAAGAAG-3′ R2: 5′-GCTACCTTTGGTAAAGCACACAGC-3	This paper	N/A
Sema3C Cy3 probes for *in situ* hybridization: anti-sense: 5′-CCACTCCCACAGACATACAG GTGAGTACGGTTGAATGTCTGAATC-3′ sense probe (negative control): 5′-UUGUACUACACAAAAGUACUG-3′	This paper	N/A

(*Continued on next page*)

Continued

REAGENT or RESOURCE	SOURCE	IDENTIFIER
Software and algorithms		
ImageJ	Schneider et al.[61]	https://imagej.net
Angiogenesis Analyzer plugin for ImageJ	Carpentier et al.[62]	http://image.bio.methods.free.fr/ImageJ/?Angiogenesis-Analyzer-for-ImageJ
Ctvol software	Bruker Corporation	https://www.bruker.com/en/products-and-solutions/preclinical-imaging/micro-ct/3d-suite-software.html
Ctan software	Bruker Corporation	https://www.bruker.com/en/products-and-solutions/preclinical-imaging/micro-ct/3d-suite-software.html
AutoDock Tools v1.5.7	Morris et al.[63]	https://autodock.scripps.edu
PyMOL Molecular Graphics System, Version 1.3	Schrödinger, LLC	https://pymol.org/2/
IBM SPSS Statistics for Windows vers. 22.0	IBM Corp	https://www.ibm.com/support/pages/spss-statistics-220-available-download

RESOURCE AVAILABILITY

Lead contact

Further information and requests for resources and reagents should be directed to and will be fulfilled by the lead contact, Xianyou Zheng (zhengxianyou@126.com).

Materials availability

This study did not generate new unique reagents.

Data and code availability

- **Data.** data reported in this paper will be shared by the lead contact upon request.
- **Code.** This paper does not report original computer code.
- **Other.** Any additional information required to reanalyze the data reported in this paper is available from the lead contact upon request.

EXPERIMENTAL MODEL AND STUDY PARTICIPANT DETAILS

Animals and SCI model for traumatic spinal injury

Animal care and all experimental protocols were approved by the Animal Care and Use Committee of Shanghai Sixth People's Hospital (approval no. DWLL2024-0519; registration no. DWSY2021-0157). Female C57BL/6J mice or Sprague-Dawley rats (12 weeks old) were initially group housed under controlled environmental conditions (22° ±1°C; 12-h light/12-h dark cycle) with free access to food and water. After SCI or control procedures (below), mice were housed individually.

Sema3c Cas-9-KO mice were purchased from GemPharmatech™ (Sema3c-KO|Strain NO.T035361; GemPharmatech™ Co., Ltd., Nanjing, China). In general, the CRISPR/Cas9 system was microinjected into the fertilized eggs of C57BL/6JGpt mice. Fertilized eggs were then transplanted to obtain positive F0-generation mice. Knockout of Sema3c was confirmed by genotyping the mice via PCR and gene sequencing.

A stable F1-generation mouse model was obtained by mating positive F0 generation mice with C57BL/6JGpt mice. Successful Sema3C deletion was confirmed by recombinant PCR (Figure S3). Genotyping primers were as follows: F1: 5′-GCATACACACATTTAATGTTGCCTG-3′; R1: 5′-CAGTGAGAGTAAGTCATGCACAGAGATC-3′; F2: 5′-CTGGTTCGGATAAAGGAAGAAGAAG-3′; R2: 5′-GCTACCTTTGGTAAAG CACACAGC-3′.

METHOD DETAILS

To induce experimental SCI, the mice/rats were first anesthetized with 1% pentobarbital sodium (60 mg/kg) via intraperitoneal (i.p.) injection. The surgical site was shaved and sterilized, and then a midline incision was made on the animal's back at the level of the T9 vertebra. The surrounding muscles were carefully retracted to expose the spinal cord by opening the vertebral plate. The anesthetized animal was placed face down on the platform of a Modified Allen's weight drop apparatus, which was adjusted to an appropriate position to enable the 10 g weight to strike the exposed spinal cord from a vertical height of 20 mm, as previously described.[64] Control sham-operated animals received the same surgical procedures, except they were not subjected to experimental SCI using the Allen apparatus.

Recombinant SEMA3C (0.12 μg/ml, 10 μl; cat. #1728-S3, R&D Systems, Minneapolis, MN, USA) and/or FPS-ZM1 (500 nM, 1 mg/kg; cat. #HY-19370, MedChemExpress, LLC, Monmouth Junction, NJ, USA) were immediately injected locally in the contused spinal cord using a microsyringe, and then subsequently injected to the lesion core which was marked by the suture once a day until day 7 post-injury. For subsequent injections, skin and muscle suture were carefully opened once a day to inject the reagents to the lesion core under anesthesia. FPS-ZM1 is a high-affinity antagonist of the receptor for advanced glycation end products (RAGE). Animals in the sham and SCI groups were injected with an equivalent volume of PBS as a control for groups receiving injection of chemicals. After surgery, penicillin (10,000 units) was injected into the mice thigh muscle for three consecutive days to prevent infection. To facilitate urination after recovery from SCI, the animals' abdomen was gently massaged for two consecutive weeks. Depending on the following experiments, mice were euthanized at the indicated days post-injury (dpi).

Cell culture and treatments

Murine microglial BV2 cells (Zhong Qiao Xin Zhou Biotechnology Co., Ltd, Shanghai, China) were cultured in high glucose Dulbecco's Modified Eagle Medium (DMEM; ThermoFisher Scientific, Waltham, MA, USA) containing 10% fetal bovine serum (FBS), and 1% penicillin/streptomycin. BV2 cells were incubated at 37°C in a humidified incubator with a 5% CO_2/95% ambient air atmosphere. Cells from passage numbers 4-10 were used for all experiments. Once confluence reached about 80%, BV2 cells were treated with lipopolysaccharide (LPS; 100 ng/ml, Sigma, Santa Clara, CA, USA) and IFN-γ (20 ng/ml; Peprotech, Cranbury, NJ, USA) for 24 hours to induce M1 polarization,[28] or IL-4 and IL-13 (both 20 ng/ml; R&D Systems, Minneapolis, MN, USA) for 24 hours to induce M2 polarization. For SEMA3C and FPS-ZM1 treatment, 0.12 μg/ml recombinant SEMA3C and 500 nM FPS-ZM1 were added to the culture medium.

Human umbilical vein endothelial cells (HUVECs) were obtained from ScienCell Research Laboratories, Inc. (cat. #8000; Carlsbad, CA, USA) and cultured in endothelial cell medium (EC medium; cat. #1001; ScienCell Research Laboratories) containing endothelial cell growth supplement (Cat. #1052; ScienCell Research Laboratories) and FBS. HUVECs were maintained at 37°C in a humidified incubator with an atmosphere of 5% CO_2/95% air. Once confluence reached about 80%, the cells were treated with recombinant SEMA3C (0.12 μg/ml) and/or recombinant VEGF-A (10 ng/ml; cat. #493-MV-025/CF, R&D Systems).[65]

Angiogenesis functional assays

We used a tube-formation assay to determine the role of SEMA3C in regulating angiogenesis *in vitro*. HUVECs (3×10^3 cells/well) were seeded into 96-well culture plates pre-coated with Matrigel™ Matrix Growth Factor Reduced (cat. #356230; BD Biosciences, Franklin Lakes, NJ, USA). The cultures were treated with recombinant SEMA3C and/or VEGF-A. After incubating the HUVECs at 37°C for 6 h, we used the widely used Angiogenesis Analyzer plugin for ImageJ[62] along with the main ImageJ app[61] to analyze the characteristics (i.e., numbers of meshes, nodes, branches, and total length) of pseudo-capillary networks.

To assess how SEMA3C affects endothelial cell migration, we used a 2-dimensional scratch-wound assay.[66] HUVECs were seeded in 6-well culture plates and grown to confluence in EC medium (ScienCell Research Laboratories, Inc.) for 24 h. The confluent monolayer was then gently "scratched" using the same yellow plastic pipette tip (200 μl tip) for all culture plates to create a cell-free gap, over which cell migration could be observed. Non-adherent cells were removed by gently washing the cultures with PBS and aspirating the suspended cells. HUVEC cultures were maintained in serum-free EC medium. The rate at which the cell-scratch wound "closed" (i.e., narrowing of the scratch-gap) was determined by capturing repeated images of the entire scratch area 6 and 12 h after creating the scratch and measuring the width of the gap.

Micro computed tomography (μCT) scans and analysis

To assess the effect of SEMA3C on functional vascularization, a known SEMA3C inhibitor,[67] 3,5,4'-tribromosalicylanilide (CAS: 87-10-5; TCI Chemicals, Portland, OR, USA), or saline was injected into the lesion core daily (20 mg/kg)(n=3/group).[68] Seven days after inducing SCI, the rats were anesthetized, and the thoracic cavity was opened to expose the heart. Subsequently, the left ventricle was first perfused with heparinized saline (100 ml), and 4% PFA (40 ml) followed by 10 ml of MICROFIL® injection compound (Flow Tech, Inc., Carver, MA, USA). Finally, the tissues were incubated overnight at 4°C. The spinal tissues were assessed using a SkyScanTM micro-CT (SkyScan-1176; Bruker Corporation, Billerica, MA, USA) at a voxel size of 4 μm. A three-dimensional (3D) reconstruction of the vessel tree was made using Ctvol software (Bruker Corporation), and the average vessel diameter and vascular volume were calculated using Ctan software (Bruker Corporation).[69]

Quantitative real-time PCR (real-time qPCR)

Total RNA was extracted from cultured cells and homogenized spinal cord tissues using an EZ-press RNA Purification Kit (cat. #B0004D-100; EZBioscience, Roseville, MN, USA). Reverse transcription was carried out using a cDNA Reverse Transcription Kit (EZBioscience) according to the manufacturer's instructions. Quantitative analysis was performed using SYBR Green I Master Mix (EZBioscience) and a LightCycler® 480 Real-time PCR system (Roche, Basel, Switzerland). The qPCR primers are listed in the key resources table. Each experiment was replicated three times, and quantitation represents the mean of three samples ±SD.

Western blot analysis

Protein extracted from cells and tissue samples was analyzed using standard western blotting procedures. Samples were centrifuged, diluted with loading buffer, and heated at 95°C for 5 min. Protein concentration was determined using a BCA protein assay kit (Cell Signaling Technology, Danvers, MA, USA). Equivalent amounts of protein (10 μg) were separated on 10%-15% SDS polyacrylamide gels.

After electrophoresis, proteins were transferred onto PVDF membranes (Millipore, Billerica, MA, USA). Membranes were blocked in 7% nonfat milk for 2 h, and then incubated at 4°C overnight with primary antibodies against SEMA3C, BAX, caspase 1, cleaved caspase 1, caspase 3, cleaved caspase 3, RAGE, NF-κB p65, phospho-NF-κB p65, NLRP3, VEGF-A, Arg-1, iba-1, iNOS, and Tuj1 (See key resources table). After washing gently in tris-buffered saline containing 0.1% Tween 20, membranes were incubated with HRP-conjugated secondary goat anti-rabbit/mouse antibodies (Jackson ImmunoResearch Labs, Shanghai, China) for 1 h at RT. GAPDH was used as the protein loading control. Blots were visualized using an ECL kit (cat. #SQ201; EpiZyme Biotechnology Ltd., Shanghai, China) and analyzed using ImageJ software.

Enzyme-linked immunosorbent assay (ELISA)

Inflammatory cytokines were assessed using ELISA kits specific for TNF-α, IL-1β, and IL-6 (Anogen, Shenzhen, Guangdong, China) and serum serotonin (Labor Diagnostika Nord GmbH & Co.KG, Nordhorn, Germany) according to manufacturer's instructions. Absorbance was read on a microplate reader at 450 nm.

Immunocytochemistry, immunohistochemistry, and histology

For histological analysis, spinal cord samples (3 mice per group/cardinal plane/time point) were embedded in paraffin and sectioned (coronal or sagittal) at a thickness of 5 μm. Sections were dewaxed using xylene, followed by rehydration using a descending series of ethanols and stained with hematoxylin for 5 min. Sections were then differentiated in 1% hydrochloric acid, counterstained with eosin for 3 min, and dehydrated with increasing series of ethanols to clearing with xylene.

For immunofluorescence, cell cultures were fixed using 4% PFA for 15 min, permeabilized with 0.3% Triton X-100 for 15 min, and blocked with 5% BSA in phosphate-buffered saline–Tween20 (PBST, 0.1% Tween20) for 1 h at RT. For paraffin sections of fresh tissue samples, mice were first perfused with PBS and 4% PFA, then tissues were harvested and postfixed in 4% PFA overnight, progressively dehydrated with ethanol to 100% ethanol, cleared in xylene, embedded in paraffin, and sectioned at a thickness of 10 μm. For frozen sections of fresh tissue samples, tissues were fixed in 4% PFA and then passed through a sucrose gradient, frozen, and sectioned on a freezing microtome. After washing with PBS, cells and tissue samples were blocked and incubated overnight with primary antibodies. Species-specific secondary antibodies tagged with a fluorophore were then applied. Cell nuclei were counterstained with DAPI (Sigma-Aldrich, St. Louis, MO, USA). Multiplex immunofluorescence was stained using tyramide tignal amplification (TSA) technique without considering whether the antibodies from the first round will cross-react with the antibodies from the second round. The main procedure was similar with traditional immunofluorescence protocol. Briefly, sections were deparaffinized, hydrated, blocked. The first primary antibody was incubated overnight. Then, the sections were incubated with corresponding HRP-labeled second antibody (Abcam, Cambridge, UK) for 50min at RT. After washing with PBST, TSA working fluid (World Advanced Science Co., Ltd, Shanghai, China) was added for 10-min incubation. Microwave treatment was used to remove the bound primary and secondary antibodies. Previous steps were repeated for the second or third primary antibody labeling. Cell nuclei were counterstained with DAPI. Immunofluorescence was imaged with a Leica epifluorescence microscope (Leica, Wetzlar, Germany), and images were acquired for analysis. The intensity of immunofluorescent staining was quantified using ImageJ software, and for presentation here, only brightness adjustments were made evenly across the entire digital image when needed to improve clarity.

In situ hybridization

In situ hybridization Cy3 probes (sense and anti-sense) for Sema3C mRNA were used to detect Sema3C expression. Mice were first perfused with PBS and RNA free PFA, then tissues were harvested and postfixed in RNA free PFA overnight. The paraffin-embedded slides (5μm) were deparaffinized in xylene, rehydrated with an ethanol gradient (absolute ethanol, 95% ethanol, 80% ethanol, 70% ethanol), digested with proteinase K at 37°C for 20 min, the reaction was terminated by addition of 0.2% glycine solution for 1min. After gently washed with PBS two times and fixed in 4% PFA for 10 min, slides were acetylated with acetic anhydride (PH=8.0) for 5min to lower the background signal. Slides were washed with 5× sodium chloride/sodium citrate buffer, prehybridized at 65°C for 1 hour, hybridized (probe dissolved with DEPC water at100uM/OD, dilute with hybridization mixture at 1:1000) at 65°C for 48 hours, and then stained with DAPI. The probes for Sema3C were as follows: 5′-CCACTCCCACAGACATACAGGTGAGTACGGTTGAATGTCTGAATC-3′; the sense probe (negative control) was 5′-UUGUA CUACACAAAAGUACUG-3′. All sections were viewed and photographed using a Nikon Eclipse Ci-fluorescence microscope (Nikon Corp., Konan, Minato-ku, Tokyo, Japan).

Cytokine antibody arrays

Spinal cord tissues were harvested at 3 dpi to assess inflammatory cytokine expression. A multiplexed Quantibody® Mouse Interleukin Array (#QAM-INT-1, RayBiotech, Inc., Norcross, GA, USA) was used according to the manufacturer's instructions for quantitative measurement of 20 different interleukins. Positive signals were visualized by using a laser scanner, and fluorescence intensities were normalized to the intensities of the internal positive controls. The SEMA3C group was compared to the SCI group (n=4) for samples with fluorescence intensity values that exceeded 300 (recommended by RayBiotech). Differentially expressed inflammatory cytokines were arranged using hierarchical clustering and presented graphically as heatmaps.

Protein-protein docking analysis

The Alphafold software tool was used to generate the predicted structure of SEMA3C and its interaction with possible ligands.[70,71] The X-ray crystal structure of RAGE (RCSB entry: 4IM8) was obtained from the Protein Data Bank. To ensure the accuracy of the docking results, the protein was prepared using AutoDock Tools v1.5.7,[71] and water molecules were manually removed from the protein-protein docking structure.[72,73] The resulting protein-protein complex was also manually optimized by removing water and adding polar hydrogen using AutoDock Tools v1.5.7. Finally, the protein-protein interactions were predicted and visualized using PyMOL (The PyMOL Molecular Graphics System, Version 1.3, Schrödinger, LLC). The SEMA3C protein was represented as a purple-colored cartoon model, while the RAGE protein was represented as a cyan-colored cartoon model. Their binding sites are presented as stick structures, respectively colored purple for SEMA3C and cyan for RAGE. When focusing on the binding region, the binding site is then shown as a representation of the protein to which it belongs.

Nissl staining

To evaluate neuronal survival, we performed Nissl staining. 4%PFA-fixed paraffin embedded sections were dewaxed and rehydrated. The sections were washed in deionized water and then immersed in a warm solution of 1% thionine at 50°C for 45 min. Then, the sections were differentiated using a 75% ethanol solution and distilled water. For cell counting, deeply stained positive cells in the defined area randomly chosen were counted. The calibration of the profile numbers was adopted to minimize unbiased data.

Morphological analysis of spinal cord myelin structure

Transmission electron microscopy (TEM) was performed to investigate the myelin sheath structure. Samples were fixed in 2.5% glutaraldehyde, embedded in EPON^{TM} resin, and sectioned at a thickness of 60 nm on an ultramicrotome. The sections were enhanced for contrast with OsO_4/uranyl acetate before observation by TEM. Myelin sheath thickness (10 myelinated axons were counted per group) was evaluated using ImageJ. Three sections were analyzed for each group.

QUANTIFICATION AND STATISTICAL ANALYSIS

Statistical analysis

All quantitative data are presented as means ± standard deviation (SD). SPSS 22.0 (IBM Corp. Released 2013. IBM SPSS Statistics for Windows, Version 22.0. Armonk, NY: IBM Corp.) was used for statistical analyses. Pearson correlations were used to assess whether SEMA3C mRNA expression was statistically associated with expression levels of its receptor, Nrp2. One-way ANOVA followed by Dunnett's test was used for multiple group comparisons, and Student's t-test was used for comparisons of two groups, as indicated in the figure legends. All experiments were repeated at least three times to support reproducibility. We considered $P < 0.05$ to be statistically significant. The P value level is indicated by asterisks in the figure legends ('*', '**', '***' signifying P value <0.05, <0.01, <0.001, respectively).